Electronic Supplementary Information

Photochromism of phenazine-2,3-diol derivatives through excited state intermolecular proton transfer based on keto–enol tautomerization

Kazuki Ohira, Kumpei Kozuka, Naoki Kaneda, Masahiro Yamamoto, Keiichi Imato and Yousuke Ooyama*

Applied Chemistry Program, Graduate School of Advanced Science and Engineering, Hiroshima University, 1-4-1 Kagamiyama, Higashi-Hiroshima 739-8527, Japan.
E-mail: yooyama@hiroshima-u.ac.jp

1. Methods

All solvents and reagents were used as received. ^{1}H NMR and ^{13}C NMR spectra were recorded using Varian-400 (400 MHz) and Varian-500 (500 MHz) FT NMR spectrometer. FT-IR spectra were recorded using a Shimadzu IRTracer-100. High-resolution mass spectral data were acquired using a Thermo Fisher Scientific LTQ Orbitrap XL. Photoabsorption spectra were recorded using Shimadzu UV-3600-plus spectrophotometers. Fluorescence spectra were measured using a Hitachi F-4500 and HORIBA FluoroMax-4 spectrophotometer. The fluorescence quantum yields (Φ_{FL}) were determined with a Hamamatsu C9920-01 instrument equipped with CCD by use of a calibrated integrating sphere system. Fluorescence decay measurements were performed using a HORIBA DeltaFlex modular fluorescence lifetime system, using a Nano LED pulsed diode excitation source (366 nm and 451 nm). Phosphorescence decay measurements were performed using HORIBA FluoroMax-4 spectrophotometer. Thermogravimetry and differential thermal analysis (TG-DTA) were conducted under nitrogen atmosphere at a heating rate of 10 °C min^{-1} using a Rigaku Thermo plus EV02 TG-DTA8122. Differential scanning calorimetric (DSC) measurements were performed under nitrogen atmosphere using a Hitachi DSC7000X. Powder X-ray diffraction measurements were performed on a Rigaku MiniFlex600-C/CM diffractometer with Cu Kα radiator.

2. Synthesis

Phenazine-2,3-diol derivatives **PD1**, **PD2**, and **PD3** were synthesized by a facile synthetic protocol as shown in Scheme S1. **PD1** was prepared by the cyclodehydration of the *o*-phenylenediamine with 2,5-dihydroxy-1,4-benzoquinone. The reactions of **PD1** with chloromethyl methyl ether gave the derivatives **PD2** and **PD3**. These dyes were successfully characterized by ^{1}H NMR, ^{13}C NMR, FTIR, and high-resolution mass spectrometric analysis.

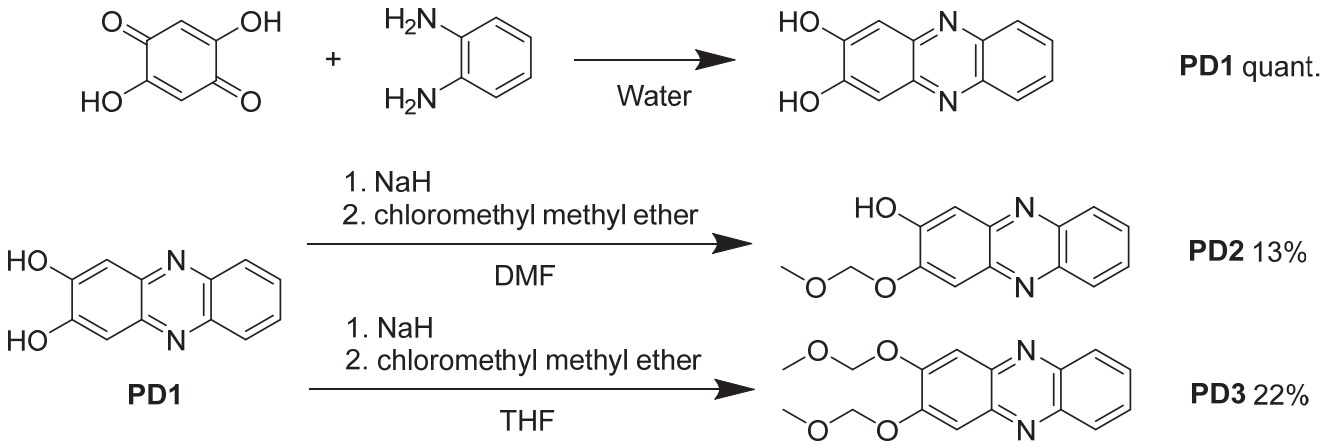

Scheme. S1 Synthetic routes of **PD1**–**3**.

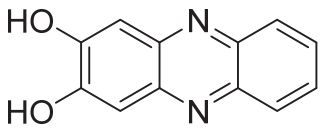

PD1 was synthesized according to procedures described in ref. S1.

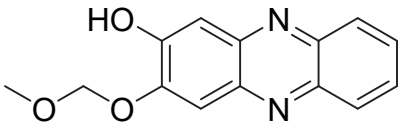

PD2 A solution of sodium hydride abt. 60 % oil suspension (41 mg) and **PD1** (218 mg, 1.03 mmol) in DMF (50 mL) was stirred at 0 °C for 30 min. Then, chloromethyl methyl ether (75 μL, 1.00 mmol) was added to the solution, and the mixture was stirred at 0 °C overnight. After concentrating under reduced pressure, the residue was chromatographed on silica gel (ethyl acetate/hexane = 1/4 as eluent). The resulting residue was dissolved in THF and subjected to reprecipitation by hexane to afford **PD2** as a white yellow solid (219 mg, 50% yield); m.p. 184 °C; IR (ATR): $\tilde{\nu}$ = 2785, 1636, 1601, 1570, 1537, 1516 cm^{-1}; ^{1}H NMR (500 MHz, acetone-d_6): δ = 9.32 (s, br, 1H, OH) 8.07–8.15 (m, 2H, aromatic), 7.74–7.85 (m, 2H, aromatic), 7.63 (s, 1H, aromatic), 7.43 (s, 1H, aromatic), 5.57 (s, 2H, CH_2), 3.57 (s, 3H, CH_3) ppm; ^{13}C NMR (125 MHz, $CDCl_3$): 152.00, 143.09, 143.07, 142.68, 142.25, 130.00, 129.92, 129.74, 129.48, 109.45, 109.09, 96.06, 56.96 ppm; HRMS (ESI): *m/z* found 257.09195 $[M+H]^+$, calculated for $C_{14}H_{13}N_2O_3$ $[M+H]^+$: 257.09207.

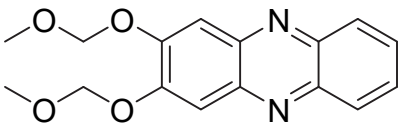

PD3 A solution of sodium hydride abt. 60 % oil suspension (83 mg) and **PD1** (216 mg, 1.02 mmol) in DMF (50 mL) was stirred at 0 °C for 30 min. Then, chloromethyl methyl ether (150 μL, 2.00 mmol) was added to the solution, and the mixture was stirred at 0 °C overnight. After concentrating under reduced pressure, the residue was chromatographed on silica gel (ethyl acetate/hexane = 1/4 as eluent). The resulting residue was dissolved in THF and subjected to reprecipitation by hexane to afford **PD3** as a white solid (158 mg, 53% yield); m.p. 137 °C; IR (ATR): $\tilde{\nu}$ = 2785, 1636, 1601, 1570, 1537, 1516 cm^{-1}; ^{1}H NMR (500 MHz, acetone-d_6): δ = 8.11–8.16 (m, 2H, aromatic), 7.80–7.84 (m, 2H, aromatic), 7.65 (s, 2H, aromatic), 5.55 (s, 4H, CH_2), 3.57 (s, 6H, CH_3) ppm; ^{13}C NMR (125 MHz, acetone-d_6): δ = 153.08, 143.13, 142.53, 130.00, 129.98, 110.17, 95.97, 56.81, 56.80 ppm; HRMS (APCI): *m/z* found 301.11872 $[M+H]^+$, calculated for $C_{16}H_{17}N_2O_4$ $[M+H]^+$: 301.11828.

3. X-Ray crystallographic analysis

The reflection data of **PZ1** and **PZ2** have been reported in Ref. S1, with the S3 Cambridge Crystallographic Data Centre (CCDC 2194829 for **PZ1** and CCDC 2194831 for **PZ2)**.

The reflection data of **PD1** (keto form) and **PD2** were collected at 100 K and 300 K on a RIGAKU XtaLAB Synergy R/DW diffractometer using Mo Kα radiation (λ = 0.71073 Å). The structures were resolved using direct methods with SHELXT 2018/2 and refined using full-matrix least-squares techniques against F^2 (SHELXL 2018/3). Hydrogen atoms were fixed geometrically and not refined. Crystallographic data have been deposited in the S3 Cambridge Crystallographic Data Centre (CCDC 2328436 (100K) and 2328438 (300 K) for **PD1** and CCDC 2328440 (100 K) and 2328442 (300K) for **PD2**).

Crystal of PD1:A suitable crystal of **PD1 (keto form)**, appearing as a dark red block and plate, was obtained through the sublimation of **PD1** black powder at a pressure of 6.7 × 10^{-2} Pa and a temperature of 235 ℃.

Crystallographic data (keto form, measured at 100 K): CCDC 2328436, $C_{12}H_8N_2O_2$, M = 212.21, monoclinic, a = 3.7249(2), b = 9.6327(4), c = 12.9466(5) Å, β = 92.843(3)°, V = 463.96(4) Å^3, D_{calcd} = 1.519 g cm^{-3}, space group $P2_1$ (no.4), Z = 2, 4946 reflections measured, 2365 unique (R_{int} = 0.0186), which were used in all calculations. The final R_1(reflections) = 0.0349 (2153) [$I > 2\sigma(I)$], wR_2(reflections) = 0.0999 (2365). GOF = 1.110 (Table S1).

Crystallographic data (keto form, measured at 300 K): CCDC 2328438, $C_{12}H_8N_2O_2$, M = 212.21, monoclinic, a = 3.7817(2), b = 9.7180(6), c = 12.9407(6) Å, β = 92.150(5)°, V = 475.24(4) Å^3, D_{calcd} = 1.483 g cm^{-3}, space group $P2_1$ (no.4), Z = 2, 2171 reflections measured, 2332 unique (R_{int} = 0.0264), which were used in all calculations. The final R_1(reflections) = 0.0466 (1698) [$I > 2\sigma(I)$], wR_2(reflections) = 0.1192 (2332). GOF = 1.043 (Table S1).

Crystal of PD2: A suitable crystal of **PD2 (enol form)**, appearing as a clear yellow needle, was recrystallized from an ethanol solvent as an air-stable, clear yellow needle crystal.

Crystallographic data (enol form, measured at 100 K): CCDC 2328440, $C_{14}H_{12}N_2O_3$, M = 256.26, monoclinic, a = 23.2329(10), b = 4.8344(2), c = 23.5477(11) Å, β = 116.157(6)°, V = 2374.0(2) Å^3, D_{calcd} = 1.434 g cm^{-3}, space group $P2_1/n$ (no.14), Z = 8, 12554 reflections measured, 5665 unique (R_{int} = 0.0326), which were used in all calculations. The final R_1(reflections) = 0.0425 (4321) [$I > 2\sigma(I)$], wR_2(reflections) = 0.1078 (5665). GOF = 1.061 (Table S1).

Crystallographic data (enol form, measured at 300 K): CCDC 2328442, $C_{14}H_{12}N_2O_3$, M = 256.26, monoclinic, a = 23.4299(13), b = 4.9040(2), c = 23.6545(14) Å, β = 115.944(7)°, V = 2444.0(3) Å^3, D_{calcd} = 1.393 g cm^{-3}, space group $P2_1/n$ (no.14), Z = 8, 5544 reflections measured, 6994 unique (R_{int} = 0.0412), which were used in all calculations. The final R_1(reflections) = 0.0490 (3855) [$I > 2\sigma(I)$], wR_2(reflections) = 0.1313 (6994). GOF = 1.003 (Table S1).

Table S1 Crystal data and structure refinement parameters for **PD1** [CCDC 2328436 (100 K) and 2328438 (300 K)] and **PD2** [CCDC 2328440 (100 K) and 2328442 (300 K)].

Compound	**PD1** (measured at 100 K)	**PD1** (measured at 300 K)	**PD2** (measured at 100 K)	**PD2** (measured at 300 K)
Molecular formula	$C_{12}H_8N_2O_2$	$C_{12}H_8N_2O_2$	$C_{14}H_{12}N_2O_3$	$C_{14}H_{12}N_2O_3$
Formula weight	212.20	212.20	256.26	256.26
Number of reflections used for unit cell determination (2θ range/°)	4946(5.26-63.55)	2171(5.25-63.73)	12554(5.21-59.81)	5544(3.85-57.77)
Temperature/K	100.00(10)	299.50(18)	100.00(10)	299.68(16)
Crystal System	monoclinic	monoclinic	monoclinic	monoclinic
Space group	$P2_1$	$P2_1$	$P2_1/n$	$P2_1/n$
a/Å	3.7249(2)	3.7817(2)	23.2329(10)	23.4299(13)
b/Å	9.6327(4)	9.7180(6)	4.8344(2)	4.9040(2)
c/Å	12.9466(5)	12.9407(6)	23.5477(11)	23.6545(14)
α/°	90	90	90	90
β/°	92.843(3)	92.150(5)	116.157(6)	115.944(7)
γ/°	90	90	90	90
V/Å^3	463.96(4)	475.24(4)	2374.0(2)	2444.0(3)
Z	2	2	8	8
D_c/g cm^{-3}	1.519	1.483	1.434	1.393
F(000)	220	220	1072	1072
Radiation	Mo-Kα (λ = 0.71073 Å)	Mo-Kα (λ = 0.71073 Å)	Mo-Kα (λ = 0.71073 Å)	Mo-Kα (λ = 0.71073 Å)
Crystal size/mm^3	0.217×0.109×0.071	0.298×0.068×0.024	0.15×0.07×0.07	0.144×0.041×0.013
Range of induces h; k; l	-5, 5; -11, 13; -19, 19	-5, 4; -10, 14; -18, 19	-31, 29; -5, 6; -24, 30	-31, 33; -7, 5; -31, 34
Reflections collected (unique)	2365	2332	5665	6994
Reflection observed with $I_0>2\sigma I_0$	2153	1698	4321	3855
Number of parameters	146	146	347	347
Final R indexes [$I_0>2\sigma I_0$]	R_1 = 0.0349, wR_2 = 0.0981	R_1 = 0.0466, wR_2 = 0.1192	R_1 = 0.0425, wR_2 = 0.1011	R_1 = 0.0490, wR_2 = 0.1105
Final R indexes [all data]	R_1 = 0.0384, wR_2 = 0.0999	R_1 = 0.0688, wR_2 = 0.1294	R_1 = 0.0610, wR_2 = 0.1078	R_1 = 0.1106, wR_2 = 0.1313
Goodness-of-fit on F^2	1.110	1.043	1.061	1.003
Max. Shift/Error in final cycle	0.000	0.000	0.001	0.001
Max. peak in final diff. map/e Å^{-3}	0.339	0.268	0.282	0.230
Min. peak in final diff. map/e Å^{-3}	-0.233	-0.235	-0.197	-0.157

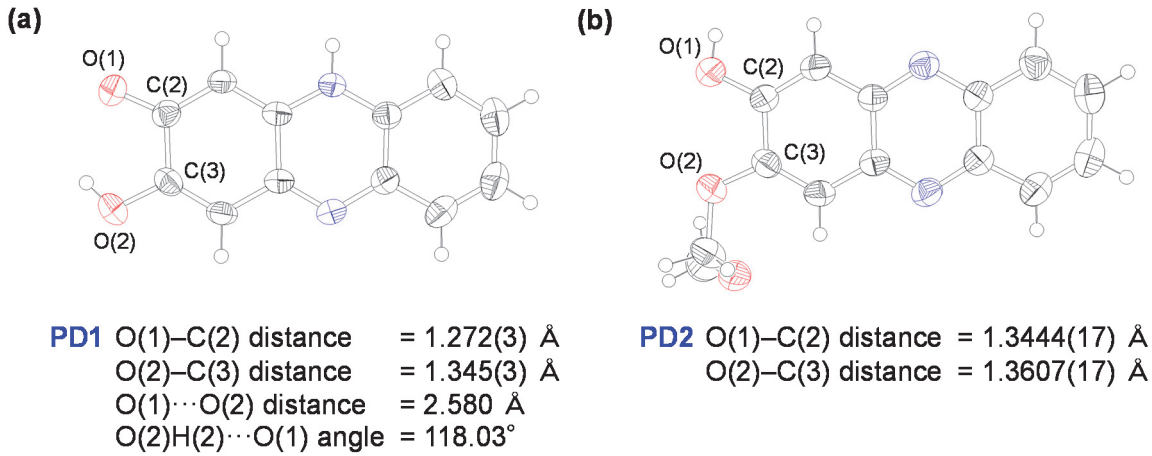

Fig. S1 X-ray crystal structures of (a) **PD1** and (b) **PD2**, measured at 300 K. Ellipsoids are shown at the 50 % probability level.

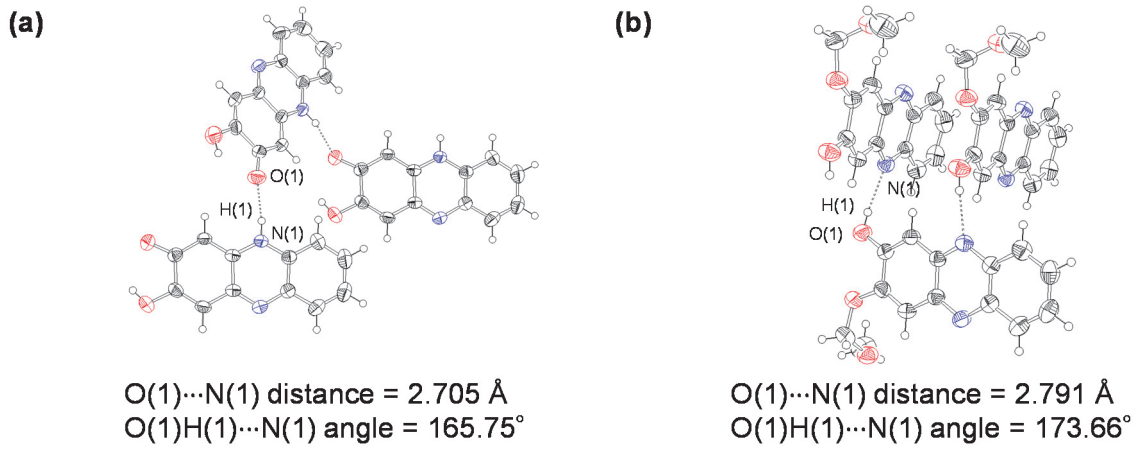

Fig. S2 Crystal packing structures of (a) **PD1** and (b) **PD2**, measured at 300 K. Ellipsoids are shown at the 50 % probability level.

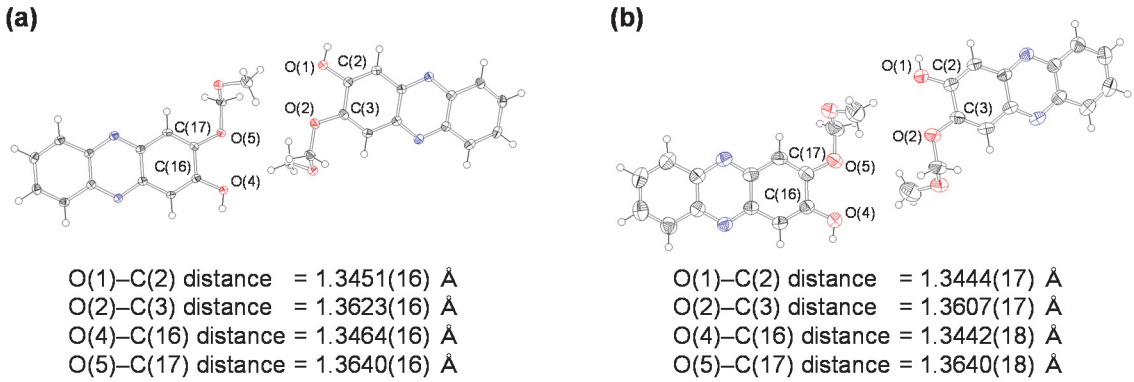

Fig. S3 X-ray crystal structures of **PD2**, measured at (a) 100 K and (b) 300 K. Ellipsoids are shown at the 50 % probability level.

4. NMR measurements

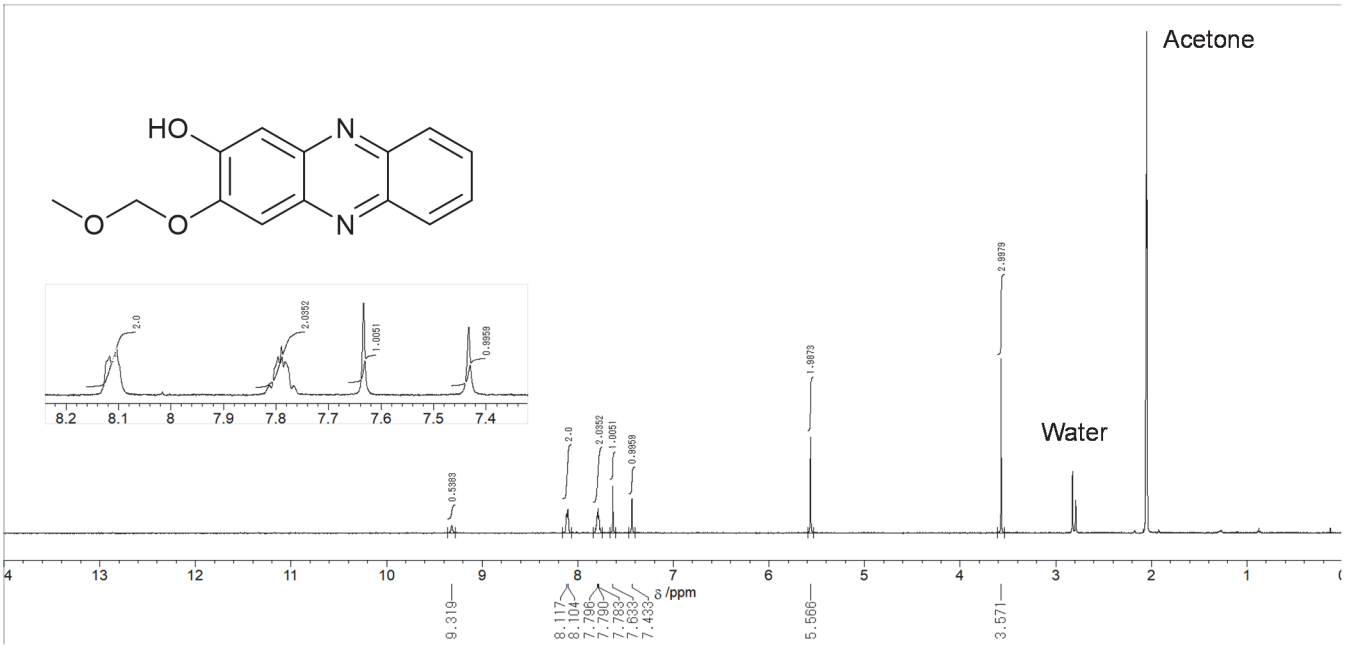

Fig. S4 ^{1}H NMR spectrum of **PD2** in Acetone-d_6.

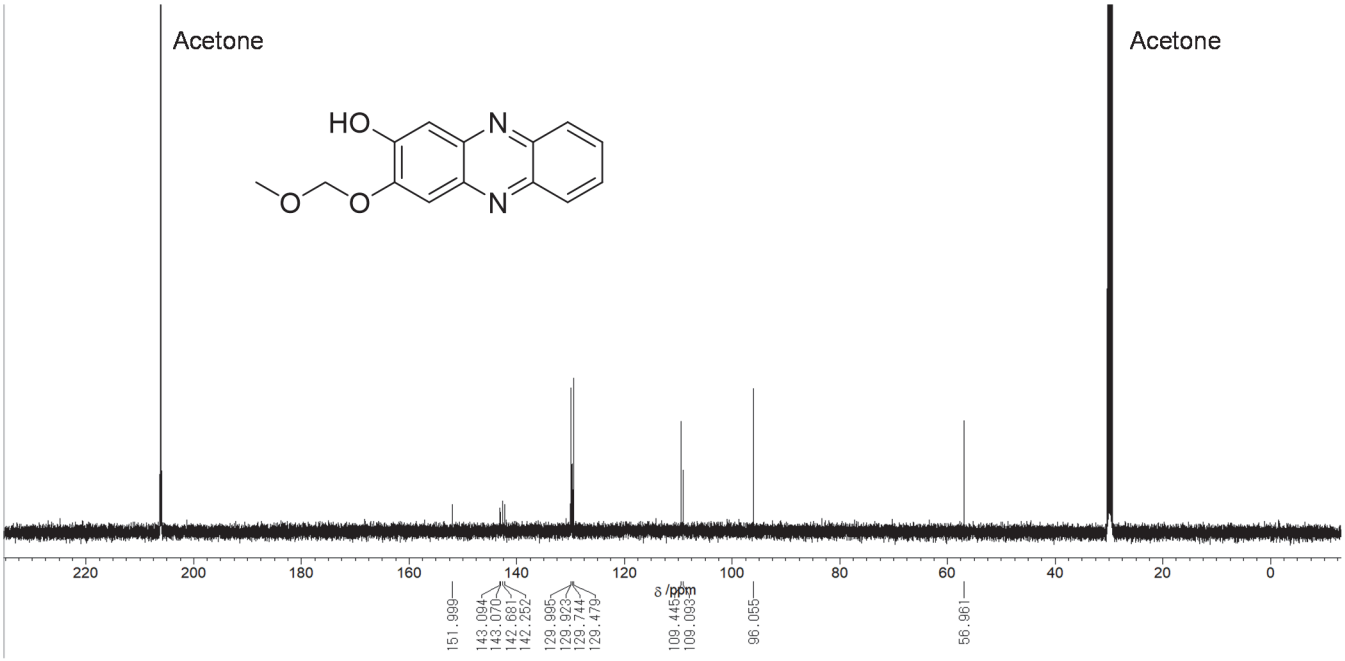

Fig. S5 ^{13}C NMR spectrum of **PD2** in Acetone-d_6.

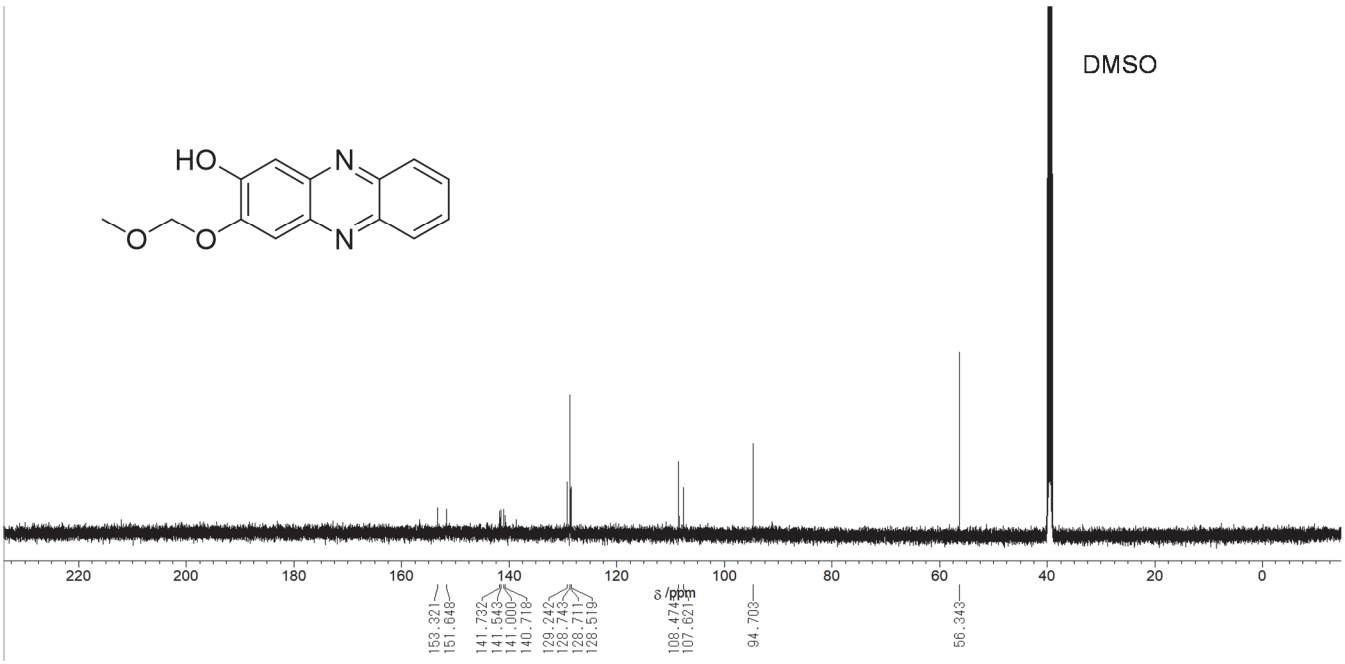

Fig. S6 ^{13}C NMR spectrum of **PD2** in DMSO-d_6.

Fig. S7 ^{1}H NMR spectrum of **PD3** in Acetone-d_6.

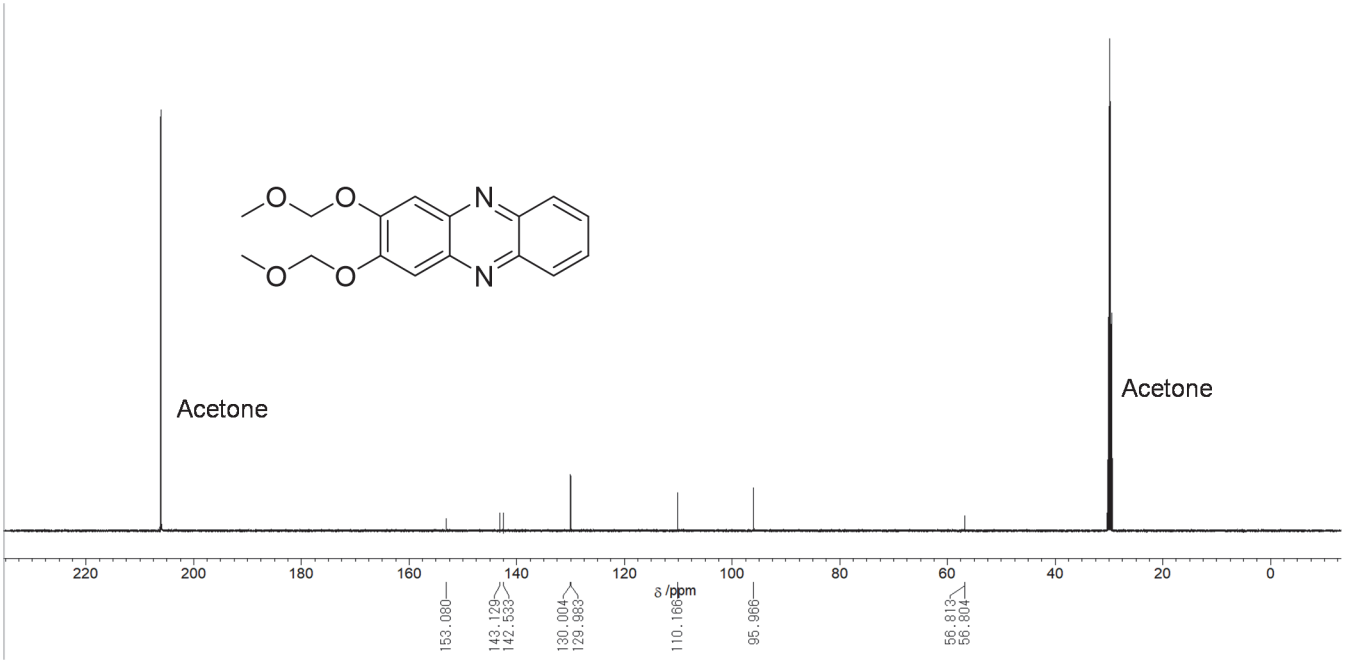

Fig. S8 ^{13}C NMR spectrum of **PD3** in Acetone-d_6.

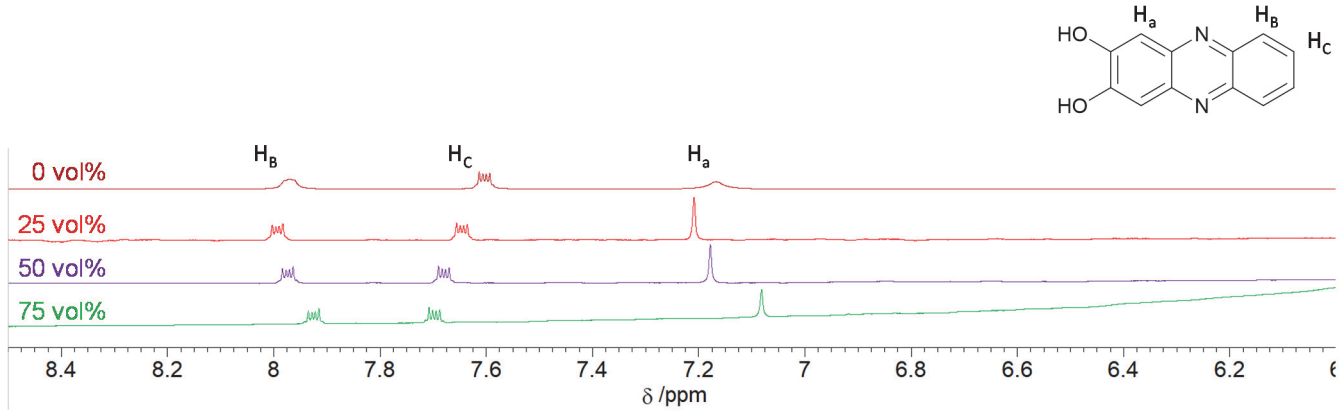

Fig. S9 ^{1}H NMR spectra of **PD1** in THF-d_8 containing H_2O (0–75 vol%). The intensity of H_A peaks doesn't change with increasing H_2O concentration (1→0.97→1.04→0.97).

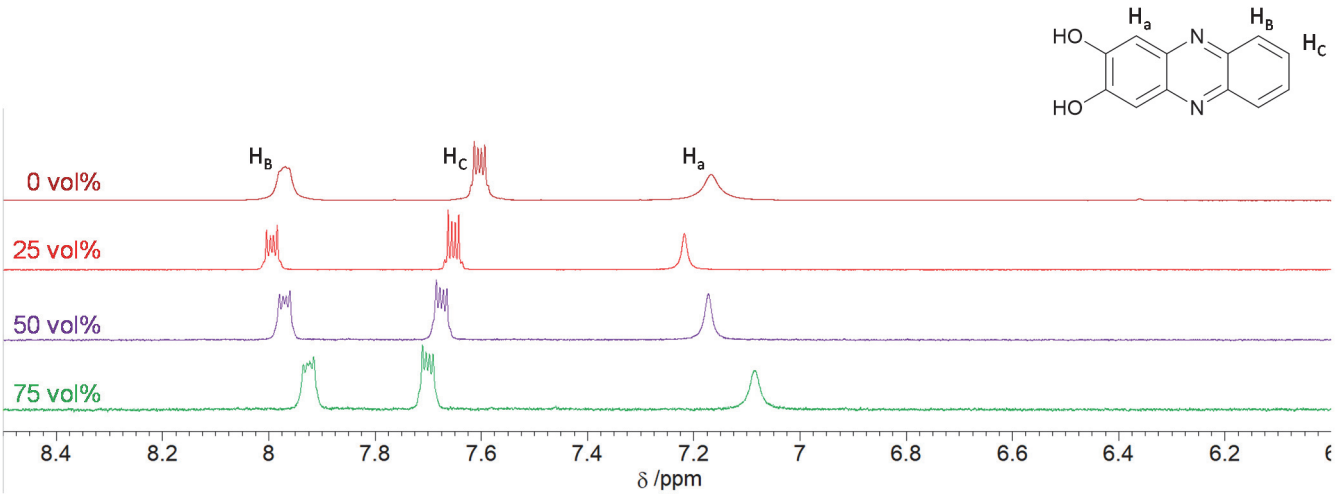

Fig. S10 ^{1}H NMR spectra of **PD1** in THF-d_8 containing D_2O (0–75 vol%). The intensity of H_A peaks decrease as increasing D_2O concentration (1→0.84→0.82→0.78). NMR measurements were performed immediately after sample preparation.

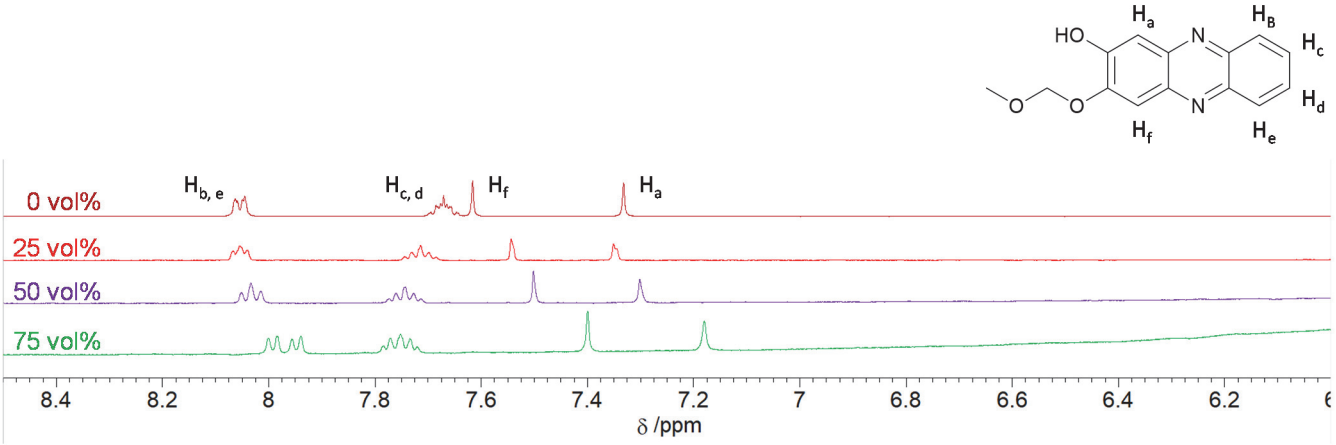

Fig. S11 ^{1}H NMR spectra of **PD2** in THF-d_8 containing H_2O (0–75 vol%). The intensities of H_A and H_F peaks don't change with increasing H_2O concentration (H_A: 1→0.98→0.92→0.88, H_F: 1→1.01→1→0.96). NMR measurements were performed immediately after sample preparation. The baseline distortion of 75 vol% spectrum is because of water.

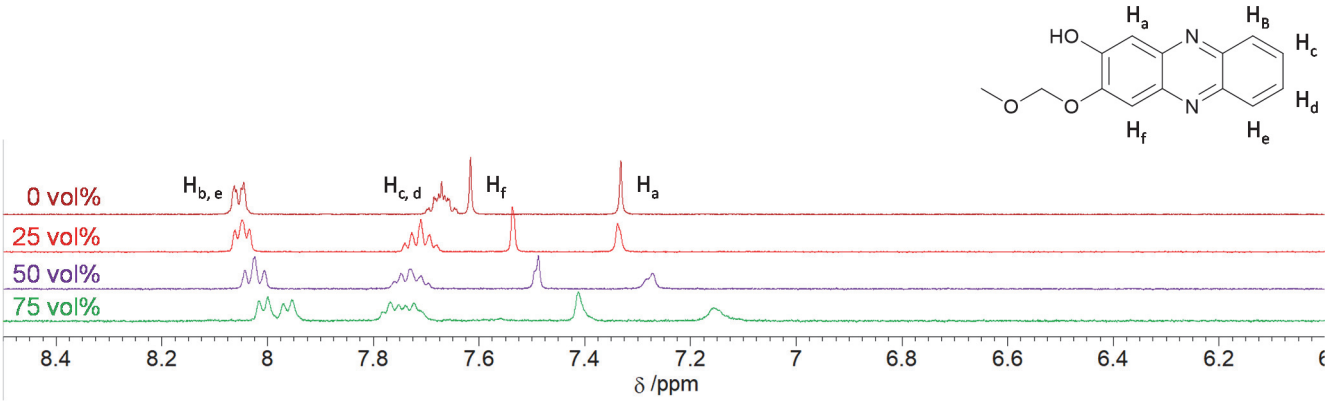

Fig. S12 ^{1}H NMR spectra of **PD2** in THF-d_8 containing D_2O (0–75 vol%). The intensity of H_A peaks decrease as increasing D_2O concentration (1→0.91→0.85→0.82) whereas that of H_F signals have no change (1 → 1.04 → 1.05 → 0.98). NMR measurements were performed immediately after sample preparation.

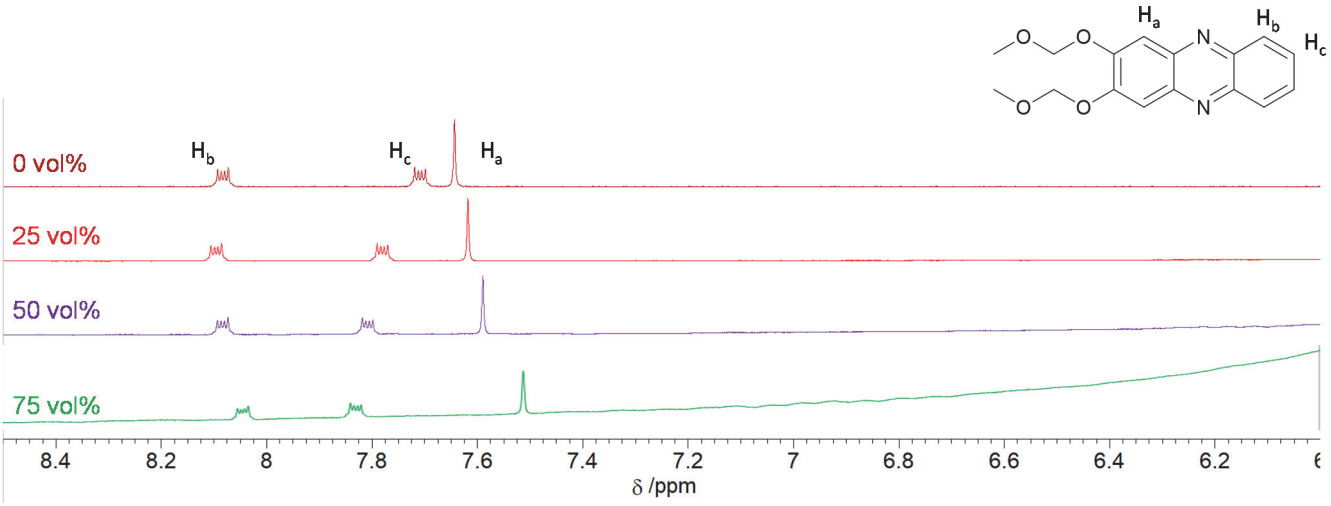

Fig. S13 ^{1}H NMR spectra of **PD3** in THF-d_8 containing H_2O (0–75 vol%). The intensity of H_A peaks doesn't change with increasing H_2O concentration (1→1.01→1.02→1.04). NMR measurements were performed immediately after sample preparation. The baseline distortion of 75 vol% spectrum is because of water.

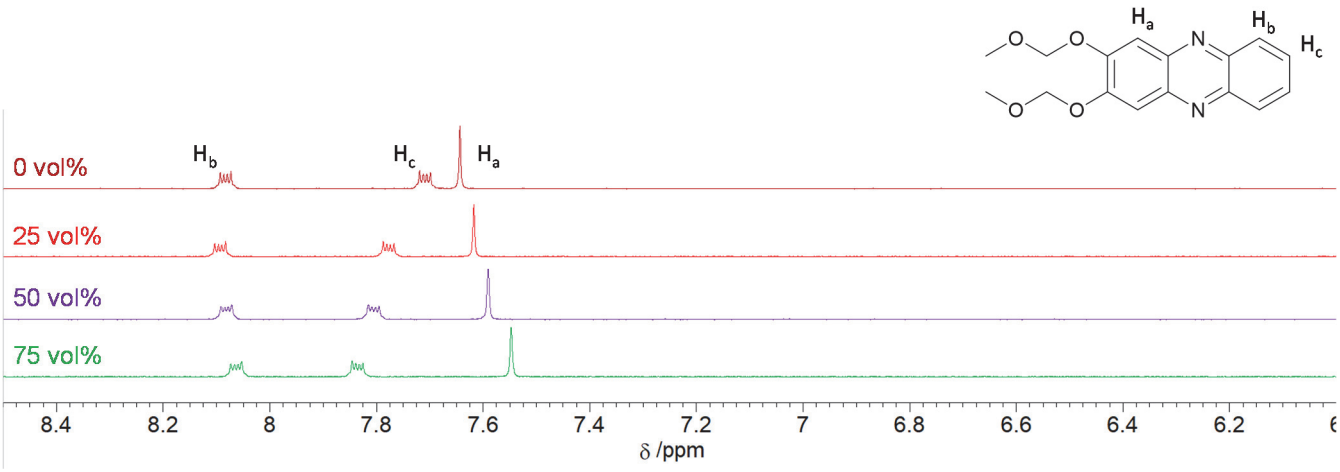

Fig. S14 ^{1}H NMR spectra of **PD3** in THF-d_8 containing D_2O (0–75 vol%). The intensity of H_A peaks doesn't change with increasing D_2O concentration (1→1.01→1.04→1.03). NMR measurements were performed immediately after sample preparation.

5. Theoretical calculations

The Gaussian 16 program[S2] was used for density functional theory (DFT) and time-dependent DFT (TD-DFT) calculations. For the convenience of calculations, the methoxymethyl groups of **PD2-E**, **PD2-K**, and **PD3** were replaced with the methoxy groups. The S_0 geometries of *anti*-**PD1-E**, *syn*-**PD1-E**, *anti*-**PD1-K**, *syn*-**PD1-K**, *anti*-**PD2-E**, *syn*-**PD2-E**, **PD2-K**, and **PD3** were optimized with frequency calculations at the B3LYP/6-311G(d,p) level. There are no imaginary frequencies for all optimized structures. The TD-DFT calculations for *anti*-**PD1-E**, *syn*-**PD1-E**, *anti*-**PD1-K**, *syn*-**PD1-K**, *anti*-**PD2-E**, *syn*-**PD2-E**, **PD2-K**, and **PD3** were performed using the optimized S_0 geometry at the B3LYP/6-311G(d,p) level.

Table S2 Cartesian coordinates of *anti*-**PD1-E**.

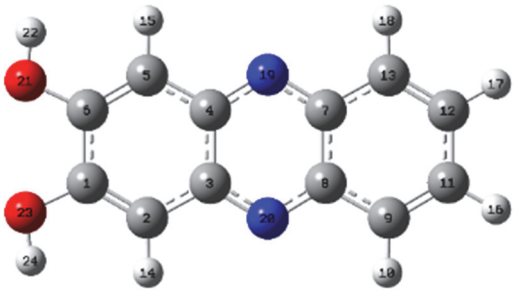

Tag	Symbol	X	Y	Z
1	C	-2.869691	-0.722496	0.000000
2	C	-1.688539	-1.408956	0.000000
3	C	-0.439022	-0.723078	0.000000
4	C	-0.439022	0.723078	0.000000
5	C	-1.688539	1.408956	0.000000
6	C	-2.869691	0.722496	0.000000
7	C	1.845435	0.720318	0.000000
8	C	1.845435	-0.720318	0.000000
9	C	3.091720	-1.410729	0.000000
10	H	3.063222	-2.493756	0.000000
11	C	4.268012	-0.712019	0.000000
12	C	4.268012	0.712019	0.000000
13	C	3.091720	1.410729	0.000000
14	H	-1.666905	-2.493455	0.000000
15	H	-1.666905	2.493455	0.000000
16	H	5.213998	-1.241560	0.000000
17	H	5.213998	1.241560	0.000000
18	H	3.063222	2.493756	0.000000
19	N	0.698276	1.420527	0.000000
20	N	0.698276	-1.420527	0.000000
21	O	-4.094720	1.301959	0.000000
22	H	-3.987983	2.259638	0.000000
23	O	-4.094720	-1.301959	0.000000
24	H	-3.987983	-2.259638	0.000000

Table S3 Cartesian coordinates of *syn*-**PD1-E**.

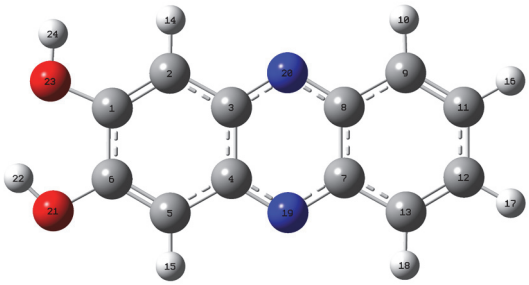

Tag	Symbol	X	Y	Z
1	C	2.850320	0.700126	0.000000
2	C	1.685421	1.405464	0.000000
3	C	0.435679	0.715991	0.000000
4	C	0.435956	-0.732199	0.000000
5	C	1.678578	-1.429944	0.000000
6	C	2.857057	-0.741554	0.000000
7	C	-1.850815	-0.719214	0.000000
8	C	-1.848053	0.721383	0.000000
9	C	-3.092117	1.415915	0.000000
10	H	-3.060835	2.498871	0.000000
11	C	-4.269987	0.720289	0.000000
12	C	-4.273484	-0.704233	0.000000
13	C	-3.099661	-1.406422	0.000000
14	H	1.667929	2.489780	0.000000
15	H	1.671990	-2.511793	0.000000
16	H	-5.214725	1.252017	0.000000
17	H	-5.221007	-1.231022	0.000000
18	H	-3.073885	-2.489438	0.000000
19	N	-0.707365	-1.422986	0.000000
20	N	-0.698665	1.417281	0.000000
21	O	4.047365	-1.386859	0.000000
22	H	4.749937	-0.723309	0.000000
23	O	4.104915	1.246081	0.000000
24	H	4.051205	2.207441	0.000000

Table S4 Cartesian coordinates of *anti*-**PD1-K**.

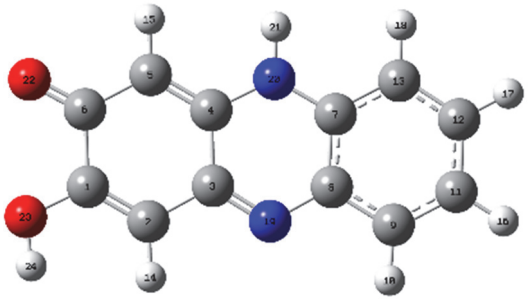

Tag	Symbol	X	Y	Z
1	C	2.943336	-0.710779	-0.000330
2	C	1.766209	-1.384980	-0.000345
3	C	0.506841	-0.695078	-0.000156
4	C	0.542708	0.778086	-0.000260
5	C	1.721941	1.464119	0.000041
6	C	3.003494	0.793179	0.000329
7	C	-1.880781	0.697945	-0.000375
8	C	-1.809634	-0.717034	0.000220
9	C	-3.009946	-1.450847	0.000714
10	H	-2.932663	-2.531141	0.001137
11	C	-4.232899	-0.805904	0.000554
12	C	-4.285115	0.596919	-0.000010
13	C	-3.121491	1.348535	-0.000503
14	H	1.721928	-2.469282	-0.000461
15	H	1.747619	2.548287	0.000197
16	H	-5.151235	-1.380243	0.000910
17	H	-5.244185	1.101493	-0.000130
18	H	-3.162563	2.433000	-0.000924
19	N	-0.605816	-1.381669	0.000110
20	N	-0.688664	1.387506	-0.000704
21	H	-0.716180	2.397828	-0.001089
22	O	4.081697	1.372422	0.001458
23	O	4.153839	-1.294045	-0.000678
24	H	4.046389	-2.252767	-0.000997

Table S5 Cartesian coordinates of *syn*-**PD1-K**.

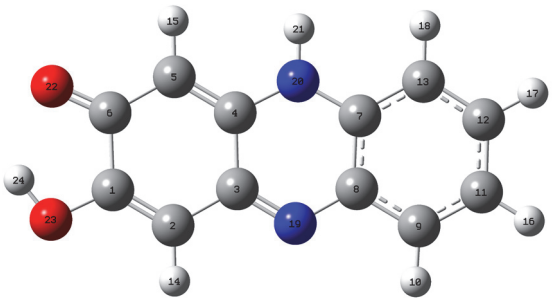

Tag	Symbol	X	Y	Z
1	C	-2.918020	-0.740562	0.000054
2	C	-1.749219	-1.428135	0.000166
3	C	-0.503009	-0.721253	0.000188
4	C	-0.543718	0.756422	0.000310
5	C	-1.725408	1.453019	0.000053
6	C	-2.971912	0.755829	-0.000084
7	C	1.877655	0.697139	0.000105
8	C	1.817219	-0.718421	0.000023
9	C	3.027447	-1.440372	-0.000186
10	H	2.961374	-2.521302	-0.000251
11	C	4.241269	-0.781828	-0.000132
12	C	4.280676	0.623220	-0.000092
13	C	3.110866	1.362790	-0.000005
14	H	-1.719393	-2.509522	0.000203
15	H	-1.748388	2.537024	-0.000199
16	H	5.165938	-1.345994	-0.000172
17	H	5.235207	1.136124	-0.000162
18	H	3.140151	2.447661	-0.000029
19	N	0.624058	-1.391740	0.000036
20	N	0.677699	1.372426	0.000158
21	H	0.696055	2.383573	-0.000081
22	O	-4.099452	1.268796	-0.000269
23	O	-4.121202	-1.312552	-0.000074
24	H	-4.741090	-0.549405	-0.000319

Table S6 Cartesian coordinates of *anti*-**PD2-E**.

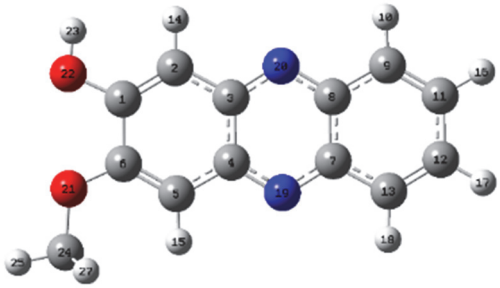

Tag	Symbol	X	Y	Z
1	C	2.462186	1.194666	0.000000
2	C	1.214428	1.748016	0.000000
3	C	0.047193	0.929357	0.000000
4	C	0.208955	-0.506769	0.000000
5	C	1.525967	-1.057716	0.000000
6	C	2.627086	-0.245353	0.000000
7	C	-2.062245	-0.757796	0.000000
8	C	-2.222425	0.673149	0.000000
9	C	-3.537333	1.220586	0.000000
10	H	-3.629748	2.300059	0.000000
11	C	-4.628972	0.395238	0.000000
12	C	-4.470616	-1.019520	0.000000
13	C	-3.223376	-1.582727	0.000000
14	H	1.074961	2.823843	0.000000
15	H	1.603673	-2.135370	0.000000
16	H	-5.627920	0.816481	0.000000
17	H	-5.351631	-1.651285	0.000000
18	H	-3.074511	-2.655880	0.000000
19	N	-0.843440	-1.325913	0.000000
20	N	-1.159535	1.496871	0.000000
21	O	3.913224	-0.653901	0.000000
22	O	3.613220	1.910633	0.000000
23	H	3.394758	2.849228	0.000000
24	C	4.168959	-2.054216	0.000000
25	H	5.252177	-2.155771	0.000000
26	H	3.754338	-2.531674	0.893845
27	H	3.754338	-2.531674	-0.893846

Table S7 Cartesian coordinates of *syn*-**PD2-E**.

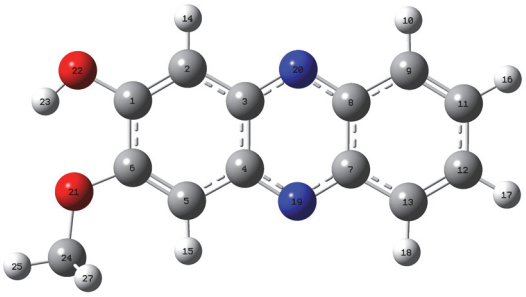

Tag	Symbol	X	Y	Z
1	C	-2.446503	-1.204204	0.000000
2	C	-1.202443	-1.762602	0.000000
3	C	-0.041697	-0.935033	0.000000
4	C	-0.200063	0.503802	0.000000
5	C	-1.516652	1.060233	0.000000
6	C	-2.601411	0.233751	0.000000
7	C	2.070104	0.758138	0.000000
8	C	2.229908	-0.672855	0.000000
9	C	3.545948	-1.219542	0.000000
10	H	3.638761	-2.298916	0.000000
11	C	4.636576	-0.393356	0.000000
12	C	4.477741	1.021836	0.000000
13	C	3.230413	1.584419	0.000000
14	H	-1.080381	-2.837594	0.000000
15	H	-1.598936	2.138005	0.000000
16	H	5.635868	-0.813866	0.000000
17	H	5.358638	1.653788	0.000000
18	H	3.081074	2.657530	0.000000
19	N	0.850668	1.324296	0.000000
20	N	1.169326	-1.497549	0.000000
21	O	-3.910168	0.613686	0.000000
22	O	-3.560629	-1.972237	0.000000
23	H	-4.324259	-1.378783	0.000000
24	C	-4.210761	2.008107	0.000000
25	H	-5.296336	2.080648	0.000000
26	H	-3.807481	2.492104	0.894406
27	H	-3.807481	2.492104	-0.894406

Table S8 Cartesian coordinates of **PD2-K**.

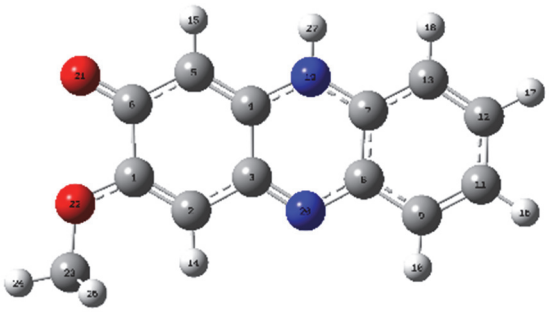

Tag	Symbol	X	Y	Z
1	C	-2.696023	-0.221255	-0.000099
2	C	-1.598523	-1.023369	-0.000143
3	C	-0.271032	-0.472451	-0.000085
4	C	-0.139416	0.994482	-0.000011
5	C	-1.234178	1.807598	-0.000016
6	C	-2.582536	1.283621	-0.000040
7	C	2.259807	0.642895	0.000036
8	C	2.029347	-0.754871	-0.000024
9	C	3.139209	-1.619088	-0.000049
10	H	2.940587	-2.683812	-0.000111
11	C	4.427447	-1.116312	-0.000003
12	C	4.637626	0.271372	0.000083
13	C	3.565826	1.149366	0.000093
14	H	-1.656801	-2.102841	-0.000239
15	H	-1.139459	2.887990	-0.000023
16	H	5.275017	-1.790781	-0.000024
17	H	5.647460	0.664694	0.000121
18	H	3.728835	2.222332	0.000139
19	N	1.152652	1.462251	0.000037
20	N	0.757842	-1.279594	-0.000088
21	O	-3.585555	1.984617	0.000004
22	O	-3.967739	-0.635448	-0.000075
23	C	-4.223432	-2.036845	0.000255
24	H	-5.306439	-2.138869	0.000682
25	H	-3.807516	-2.512417	-0.893915
26	H	-3.806826	-2.512149	0.894240
27	H	1.293302	2.463048	0.000066

Table S9 Cartesian coordinates of **PD3**.

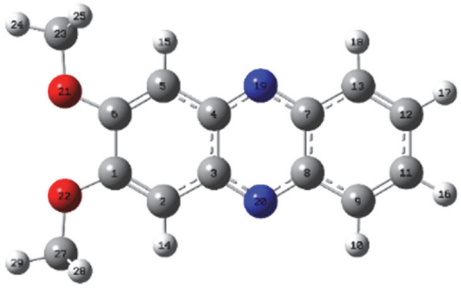

Tag	Symbol	X	Y	Z
1	C	2.331217	-0.727254	0.000000
2	C	1.148928	-1.413916	0.000000
3	C	-0.099957	-0.722035	0.000000
4	C	-0.099957	0.722035	0.000000
5	C	1.148928	1.413916	0.000000
6	C	2.331217	0.727254	0.000000
7	C	-2.384708	0.719632	0.000000
8	C	-2.384708	-0.719632	0.000000
9	C	-3.630098	-1.410089	0.000000
10	H	-3.601690	-2.493159	0.000000
11	C	-4.807276	-0.711599	0.000000
12	C	-4.807276	0.711599	0.000000
13	C	-3.630098	1.410089	0.000000
14	H	1.108244	-2.493577	0.000000
15	H	1.108244	2.493577	0.000000
16	H	-5.753013	-1.241626	0.000000
17	H	-5.753013	1.241626	0.000000
18	H	-3.601690	2.493159	0.000000
19	N	-1.235962	1.419826	0.000000
20	N	-1.235962	-1.419826	0.000000
21	O	3.562547	1.279919	0.000000
22	O	3.562547	-1.279919	0.000000
23	C	3.657388	2.699946	0.000000
24	H	4.722114	2.923992	0.000000
25	H	3.191368	3.127760	-0.893674
26	H	3.191369	3.127760	0.893674
27	C	3.657388	-2.699946	0.000000
28	H	3.191369	-3.127760	-0.893674
29	H	4.722114	-2.923992	0.000000
30	H	3.191368	-3.127760	0.893674

Table S10 Cartesian coordinates of *anti*-**PZ1**.

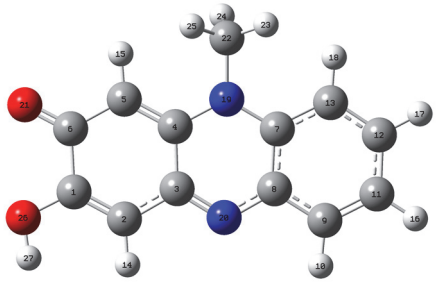

Tag	Symbol	X	Y	Z
1	C	-3.01329	-0.85481	0.008706
2	C	-1.84401	-1.53534	0.071829
3	C	-0.57355	-0.86255	0.057195
4	C	-0.56729	0.608948	0.011604
5	C	-1.74836	1.296425	-0.07371
6	C	-3.04102	0.64152	-0.08469
7	C	1.846161	0.468344	0.013246
8	C	1.729849	-0.94733	0.032746
9	C	2.893695	-1.73684	-0.00441
10	H	2.757881	-2.81103	0.020344
11	C	4.145401	-1.15814	-0.07638
12	C	4.252973	0.237572	-0.1212
13	C	3.125781	1.043896	-0.07993
14	H	-1.80716	-2.61885	0.121194
15	H	-1.79361	2.372707	-0.15256
16	H	5.034878	-1.77544	-0.10749
17	H	5.228797	0.703061	-0.19785
18	H	3.249121	2.115371	-0.14571
19	N	0.675988	1.217426	0.082158
20	N	0.514998	-1.58226	0.082579
21	O	-4.10397	1.243801	-0.16789
22	C	0.72866	2.67241	0.201816
23	H	1.664235	2.971053	0.66527
24	H	0.63195	3.159445	-0.77349
25	H	-0.08659	3.003575	0.843655
26	O	-4.23222	-1.42255	0.012843
27	H	-4.13687	-2.38075	0.072895

Table S11 Cartesian coordinates of *syn*-**PZ1**.

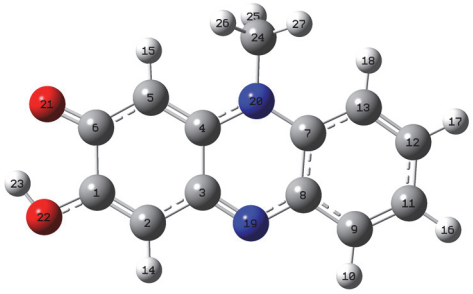

Tag	Symbol	X	Y	Z
1	C	2.986276	-0.88869	-0.01034
2	C	1.823981	-1.57973	-0.07106
3	C	0.567697	-0.88619	-0.05648
4	C	0.568106	0.590367	-0.01071
5	C	1.754184	1.284223	0.07027
6	C	3.010939	0.599749	0.074651
7	C	-1.84467	0.471773	-0.01132
8	C	-1.7399	-0.94464	-0.03404
9	C	-2.91369	-1.72364	-0.00128
10	H	-2.78777	-2.79885	-0.02869
11	C	-4.15762	-1.1323	0.070187
12	C	-4.2525	0.265835	0.118809
13	C	-3.11884	1.061015	0.080932
14	H	1.797706	-2.66028	-0.1158
15	H	1.802204	2.359958	0.149494
16	H	-5.05365	-1.74022	0.098219
17	H	-5.22417	0.739709	0.195579
18	H	-3.23291	2.133249	0.1497
19	N	-0.53565	-1.5893	-0.08303
20	N	-0.66535	1.207597	-0.07435
21	O	4.125527	1.136339	0.14734
22	O	4.196988	-1.44775	-0.00974
23	H	4.80714	-0.68073	0.055667
24	C	-0.70752	2.665508	-0.18847
25	H	-0.59881	3.14539	0.788573
26	H	0.103315	2.99308	-0.83704
27	H	-1.64483	2.972137	-0.64188

Table S12 Cartesian coordinates of **PZ2**.

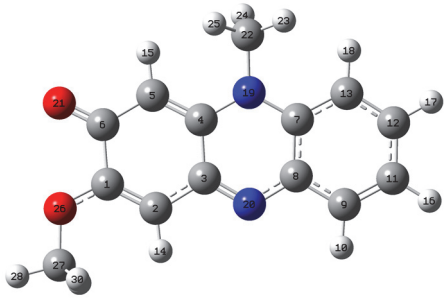

Tag	Symbol	X	Y	Z
1	C	2.800432	-0.30911	0.009061
2	C	1.726784	-1.13691	-0.0528
3	C	0.380505	-0.62831	-0.04508
4	C	0.181064	0.829225	-0.00949
5	C	1.262255	1.664119	0.074815
6	C	2.628768	1.181763	0.093926
7	C	-2.19363	0.376159	-0.01688
8	C	-1.89339	-1.0121	-0.02595
9	C	-2.94439	-1.94616	0.01383
10	H	-2.66961	-2.99364	-0.00284
11	C	-4.26145	-1.53532	0.078203
12	C	-4.55043	-0.16554	0.11264
13	C	-3.53755	0.780571	0.068778
14	H	1.812389	-2.21369	-0.09627
15	H	1.167852	2.737776	0.146768
16	H	-5.06281	-2.26332	0.111218
17	H	-5.5789	0.169258	0.18318
18	H	-3.79951	1.827339	0.126614
19	N	-1.13059	1.270781	-0.08815
20	N	-0.60547	-1.48343	-0.06829
21	O	3.600497	1.921824	0.177376
22	C	-1.37126	2.705523	-0.218
23	H	-2.33606	2.877186	-0.68608
24	H	-1.34211	3.207746	0.754012
25	H	-0.60346	3.135617	-0.85981
26	O	4.085293	-0.68396	0.01216
27	C	4.381266	-2.0752	-0.06033
28	H	5.46668	-2.14726	-0.04881
29	H	3.966345	-2.61087	0.799762
30	H	3.991392	-2.51271	-0.98528

Table S13 Excitation energy, oscillator strength, main transition orbital, and their contribution calculated for singlet states of **PD1**–**3**, **PZ1**, and **PZ2** derived from TD-DFT calculations at B3LYP/6-311G(d,p) level.

Dye	State	Excitation energy / eV	Oscillator strength	Main transition orbital	contribution	Transition
anti-**PD1-E**	S_1	3.22	0.025	HOMO→LUMO	0.98	ππ*
	S_2	3.22	0.0012	HOMO-2→LUMO	0.99	nπ*
	S_3	3.62	0.25	HOMO-1→LUMO	0.84	ππ*
				HOMO→LUMO+1	0.16	ππ*
syn-**PD1-E**	S_1	3.20	0.0012	HOMO-2→LUMO	0.99	nπ*
	S_2	3.20	0.037	HOMO→LUMO	0.97	ππ*
	S_3	3.65	0.23	HOMO-1→LUMO	0.83	ππ*
				HOMO→LUMO+1	0.16	ππ*
anti-**PD1-K**	S_1	2.84	0.13	HOMO-1→LUMO	0.23	ππ*
				HOMO→LUMO	0.75	ππ*
	S_2	2.88	0.00	HOMO-2→LUMO	0.97	nπ*
	S_3	3.41	0.30	HOMO-1→LUMO	0.72	ππ*
				HOMO→LUMO	0.19	ππ*
syn-**PD1-K**	S_1	2.90	0.039	HOMO-1→LUMO	0.71	ππ*
				HOMO→LUMO	0.27	ππ*
	S_2	3.24	0.40	HOMO-1→LUMO	0.26	ππ*
				HOMO→LUMO	0.65	ππ*
	S_3	3.40	0.00	HOMO-2→LUMO	0.97	nπ*
anti-**PD2-E**	S_1	3.24	0.021	HOMO→LUMO	0.98	ππ*
	S_2	3.24	0.0012	HOMO-2→LUMO	0.99	nπ*
	S_3	3.59	0.28	HOMO-1→LUMO	0.85	ππ*
				HOMO→LUMO+1	0.15	ππ*
syn-**PD2-E**	S_1	3.22	0.036	HOMO→LUMO	0.97	ππ*
	S_2	3.22	0.0012	HOMO-2→LUMO	0.99	nπ*
	S_3	3.64	0.25	HOMO-1→LUMO	0.84	ππ*
				HOMO→LUMO+1	0.16	ππ*
PD2-K	S_1	2.86	0.13	HOMO-1→LUMO	0.23	ππ*
				HOMO→LUMO	0.74	ππ*
	S_2	2.89	0.00	HOMO-2→LUMO	0.97	nπ*
	S_3	3.38	0.32	HOMO-1→LUMO	0.72	ππ*
				HOMO→LUMO	0.20	ππ*
PD3	S_1	3.26	0.016	HOMO→LUMO	0.97	ππ*
	S_2	3.26	0.0012	HOMO-2→LUMO	0.99	nπ*
	S_3	3.58	0.30	HOMO-1→LUMO	0.86	ππ*
				HOMO→LUMO+1	0.14	ππ*
anti-**PZ1**	S_1	2.86	0.12	HOMO-1→LUMO	0.21	ππ*
				HOMO→LUMO	0.68	ππ*

Dye	State	Excitation energy / eV	Oscillator strength	Main transition orbital	contribution	Transition
	S_2	2.90	0.01	HOMO-2→LUMO	0.88	nπ*
	S_3	3.40	0.29	HOMO-1→LUMO	0.71	ππ*
				HOMO→LUMO	0.20	ππ*
syn-**PZ1**	S_1	2.91	0.042	HOMO-1→LUMO	0.71	ππ*
				HOMO→LUMO	0.27	ππ*
	S_2	3.23	0.39	HOMO-1→LUMO	0.25	ππ*
				HOMO→LUMO	0.66	ππ*
	S_3	3.40	0.0019	HOMO-2→LUMO	0.97	nπ*
PZ2	S_1	2.87	0.12	HOMO-2→LUMO	0.11	nπ*
				HOMO-1→LUMO	0.20	ππ*
				HOMO→LUMO	0.66	ππ*
	S_2	2.91	0.017	HOMO-2→LUMO	0.85	nπ*
	S_3	3.37	0.30	HOMO-1→LUMO	0.72	ππ*
				HOMO→LUMO	0.20	ππ*

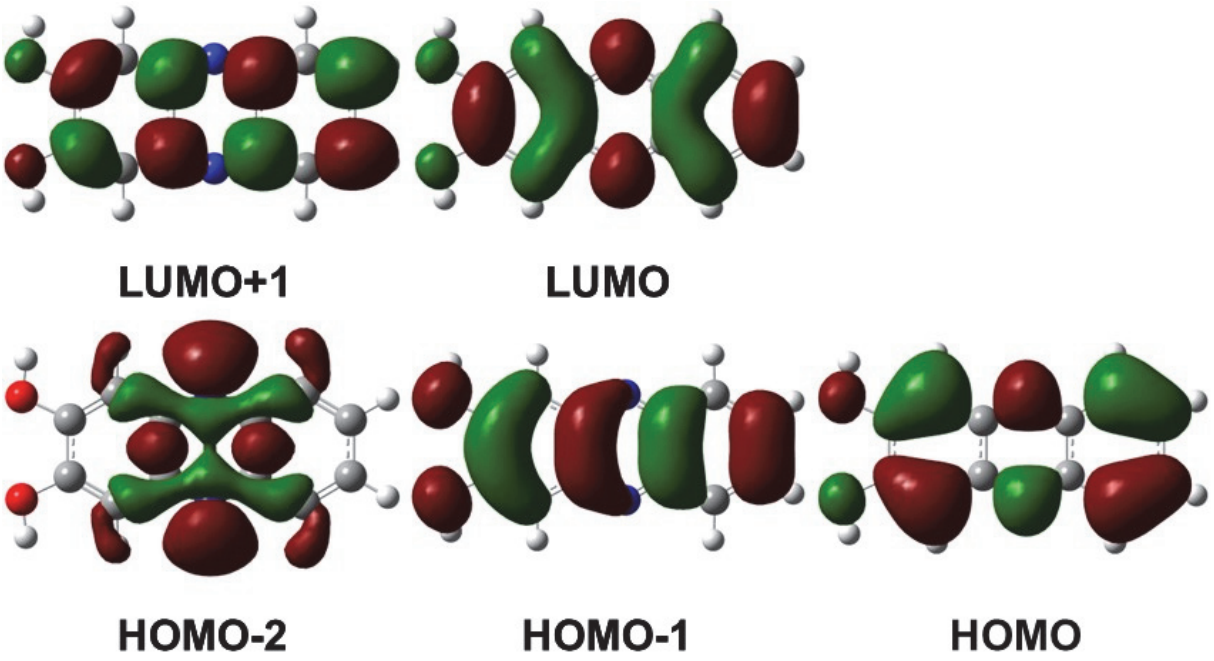

Fig. S15 Plots of visualized orbitals based on the optimized geometry of *anti*-**PD1-E** derived from DFT calculations at B3LYP/6-311G(d,p) level.

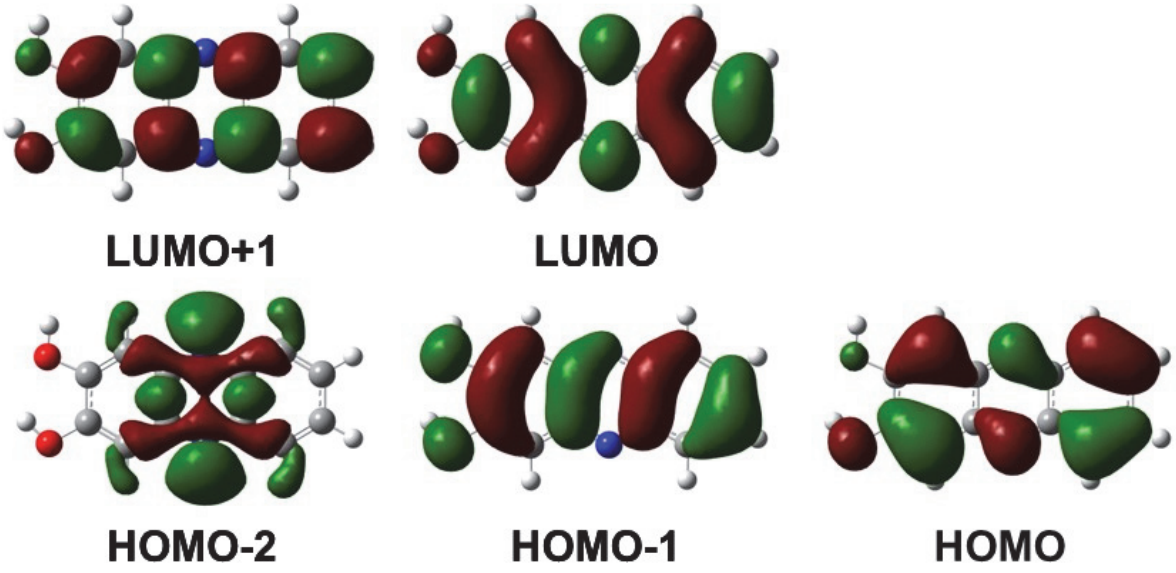

Fig. S16 Plots of visualized orbitals based on the optimized geometry of *syn*-**PD1-E** derived from DFT calculations at B3LYP/6-311G(d,p) level.

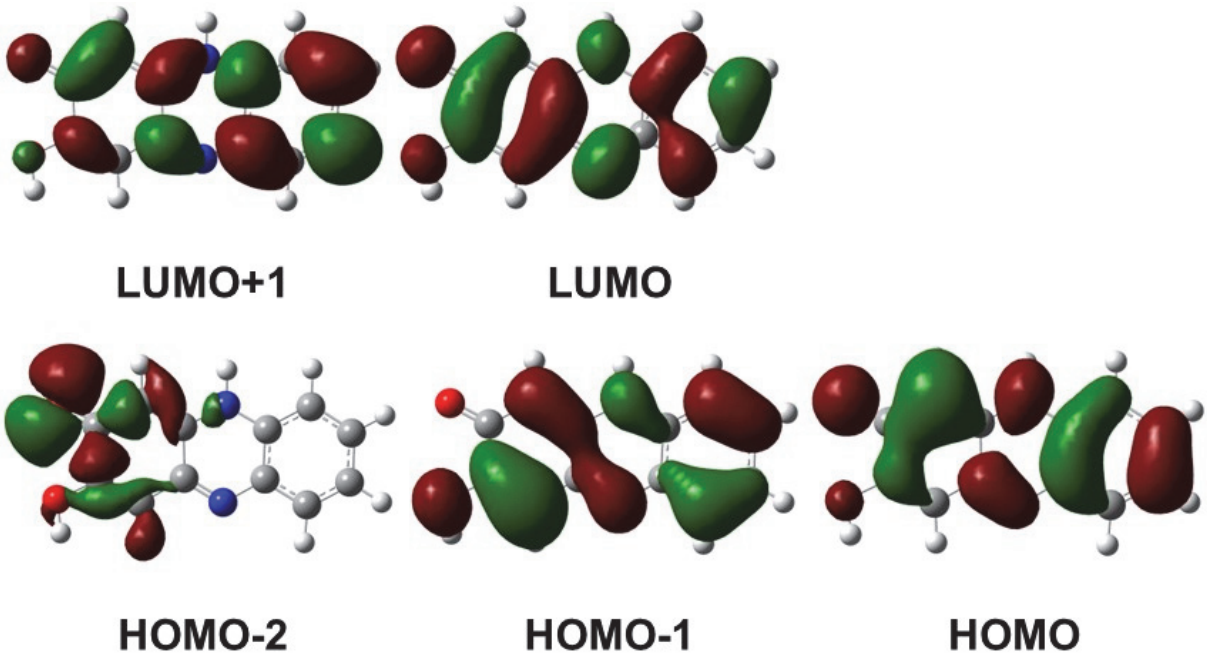

Fig. S17 Plots of visualized orbitals based on the optimized geometry of *anti*-**PD1-K** derived from DFT calculations at B3LYP/6-311G(d,p) level.

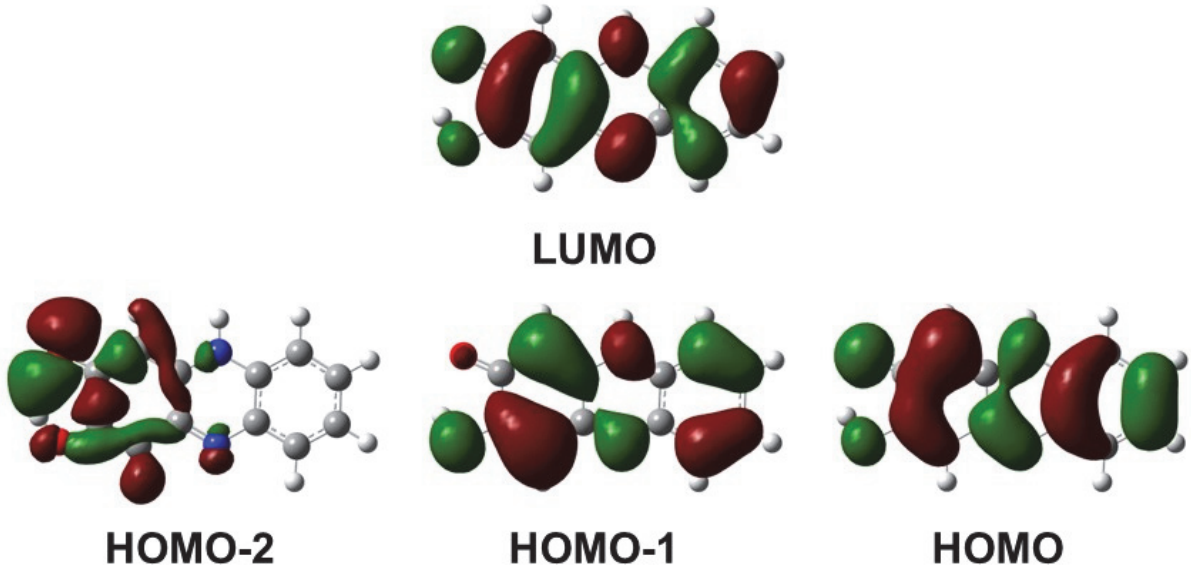

Fig. S18 Plots of visualized orbitals based on the optimized geometry of *syn*-**PD1-K** derived from DFT calculations at B3LYP/6-311G(d,p) level.

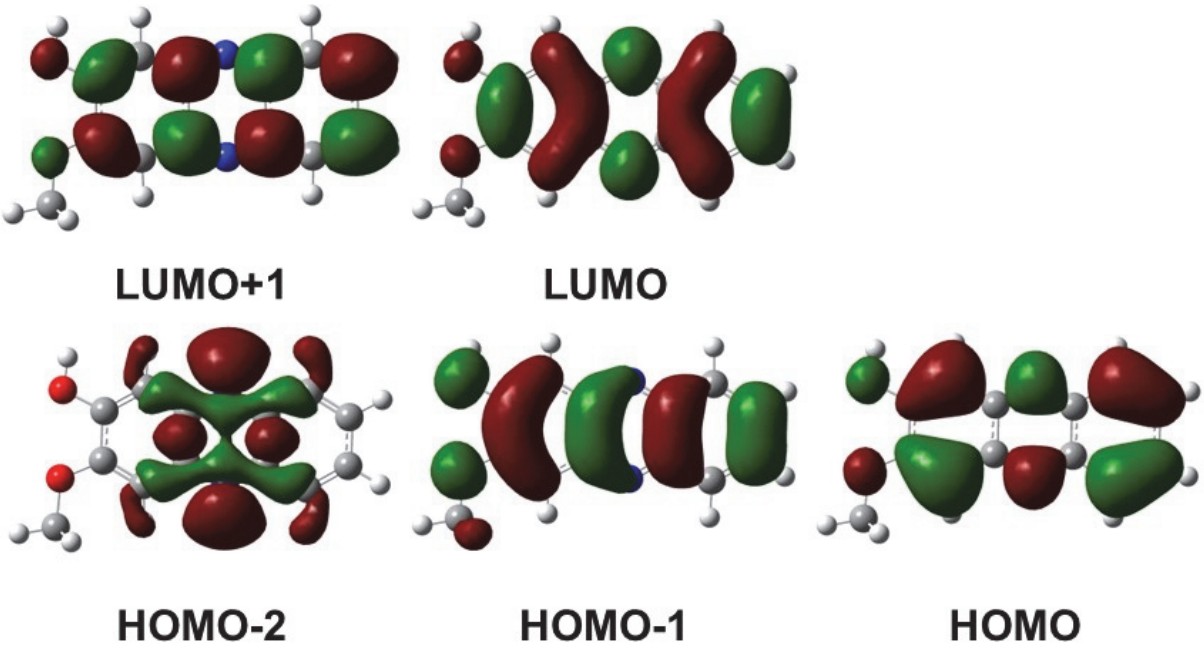

Fig. S19 Plots of visualized orbitals based on the optimized geometry of *anti*-**PD2-E** derived from DFT calculations at B3LYP/6-311G(d,p) level.

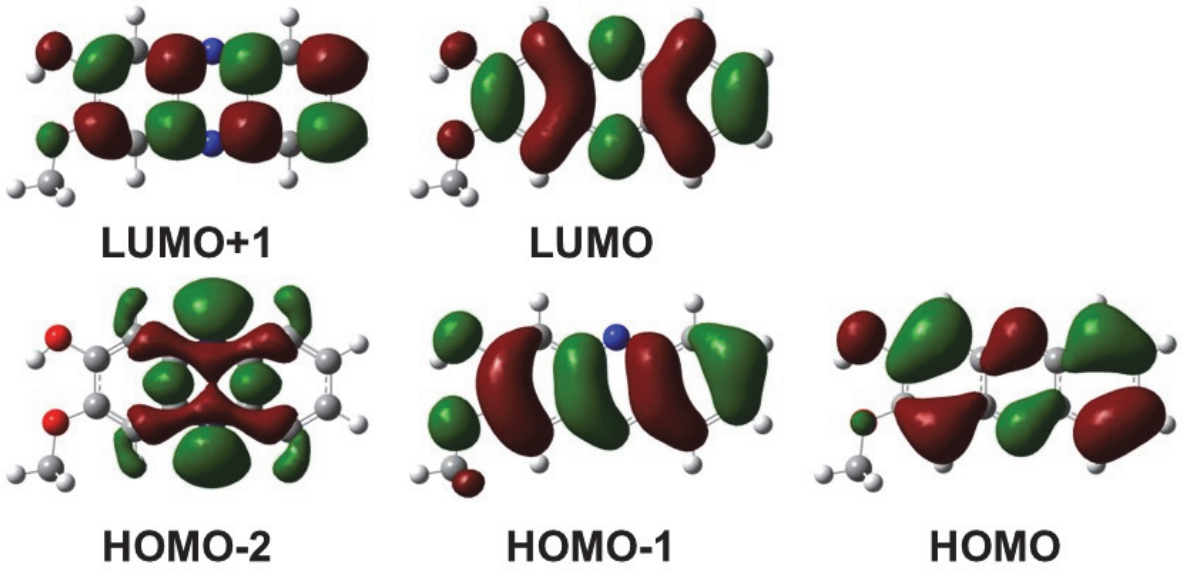

Fig. S20 Plots of visualized orbitals based on the optimized geometry of *syn*-**PD2-E** derived from DFT calculations at B3LYP/6-311G(d,p) level.

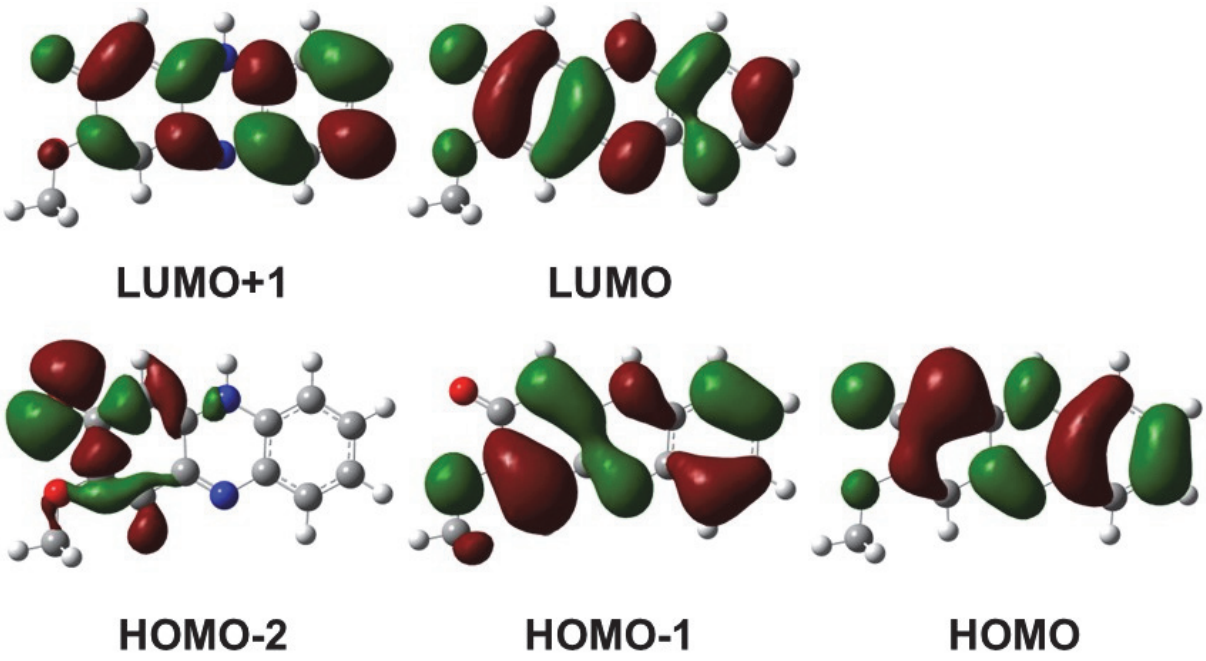

Fig. S21 Plots of visualized orbitals based on the optimized geometry of **PD2-K** derived from DFT calculations at B3LYP/6-311G(d,p) level.

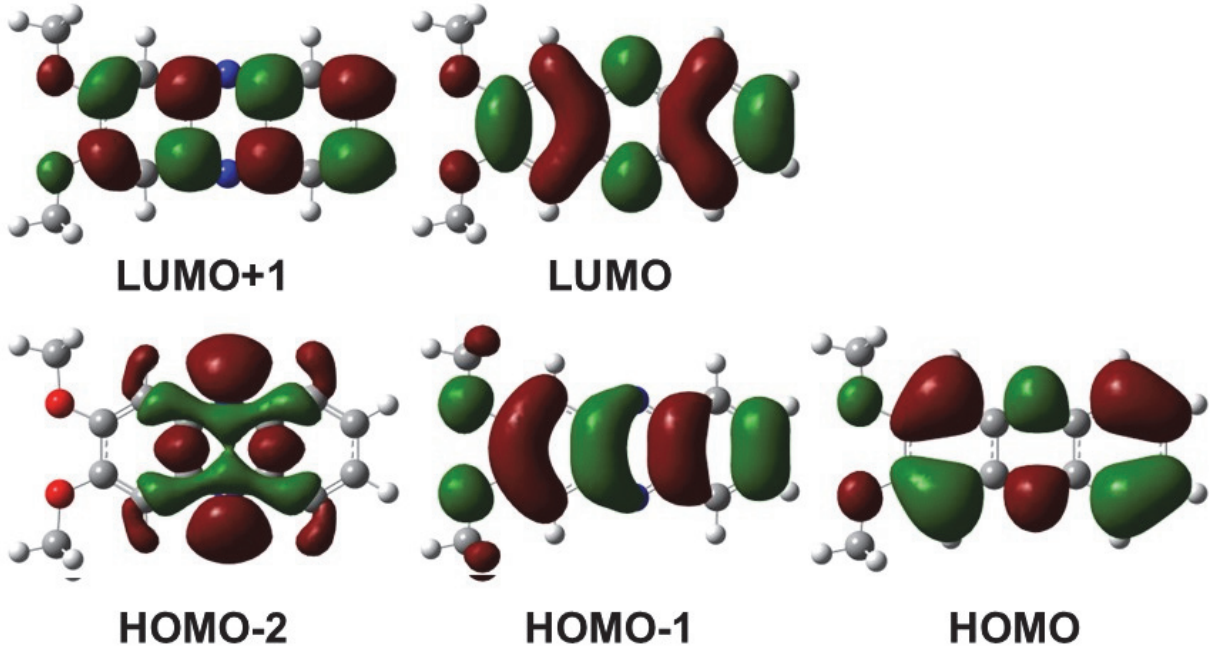

Fig. S22 Plots of visualized orbitals based on the optimized geometry of **PD3** derived from DFT calculations at B3LYP/6-311G(d,p) level.

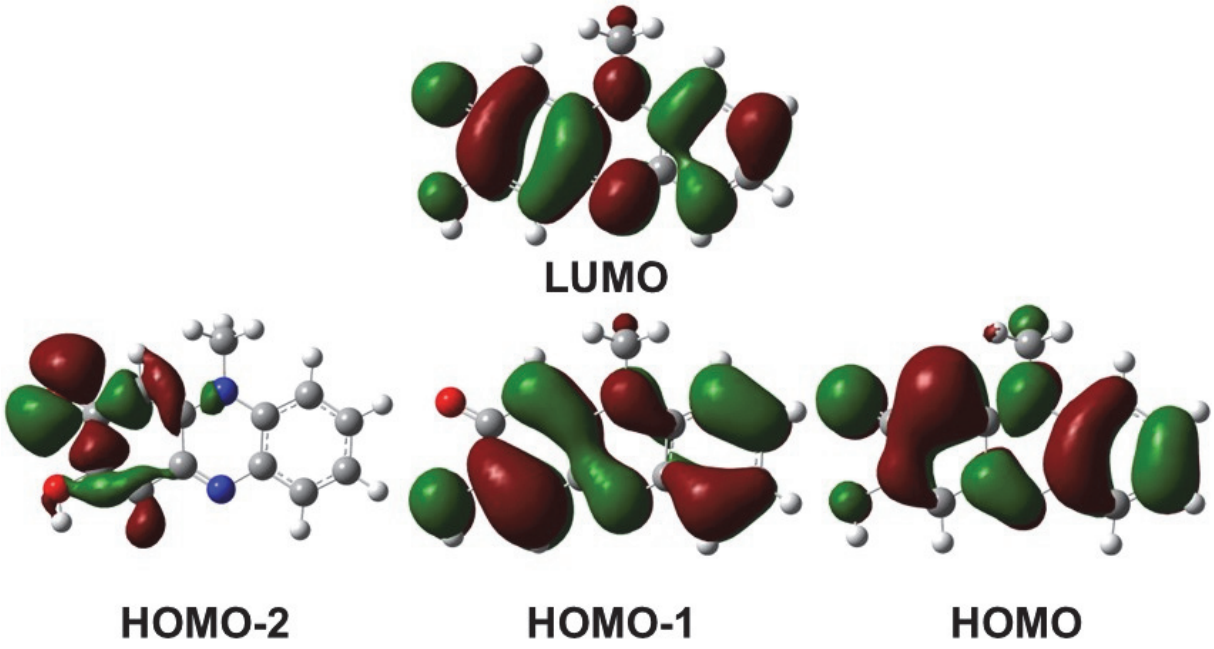

Fig. S23 Plots of visualized orbitals based on the optimized geometry of *anti*-**PZ1** derived from DFT calculations at B3LYP/6-311G(d,p) level.

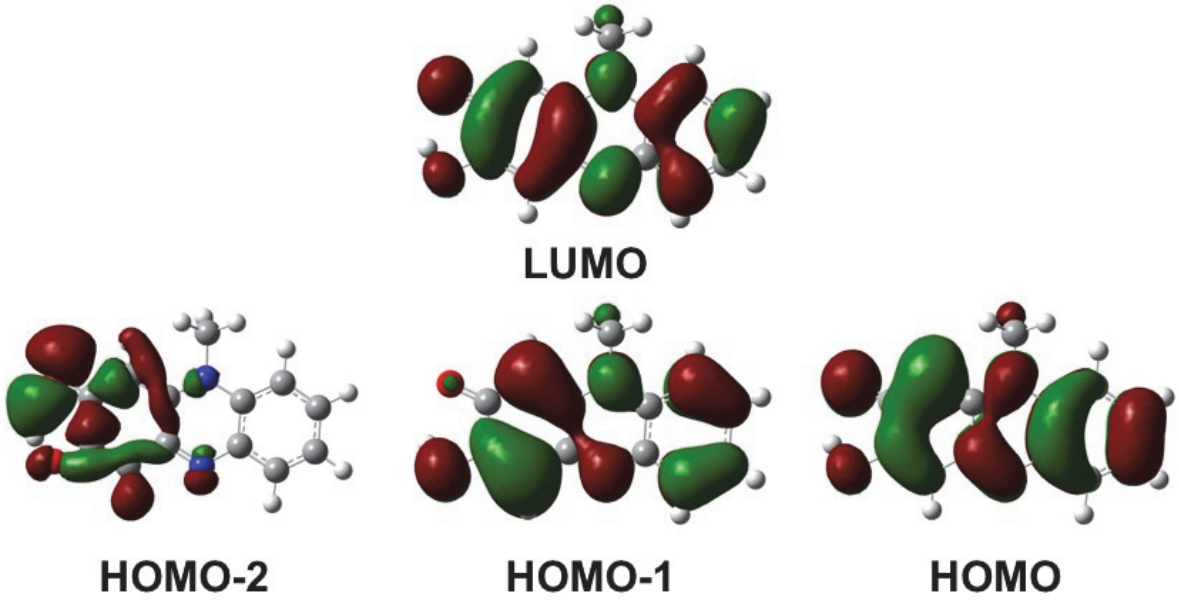

Fig. S24 Plots of visualized orbitals based on the optimized geometry of *syn*-**PZ1** derived from DFT calculations at B3LYP/6-311G(d,p) level.

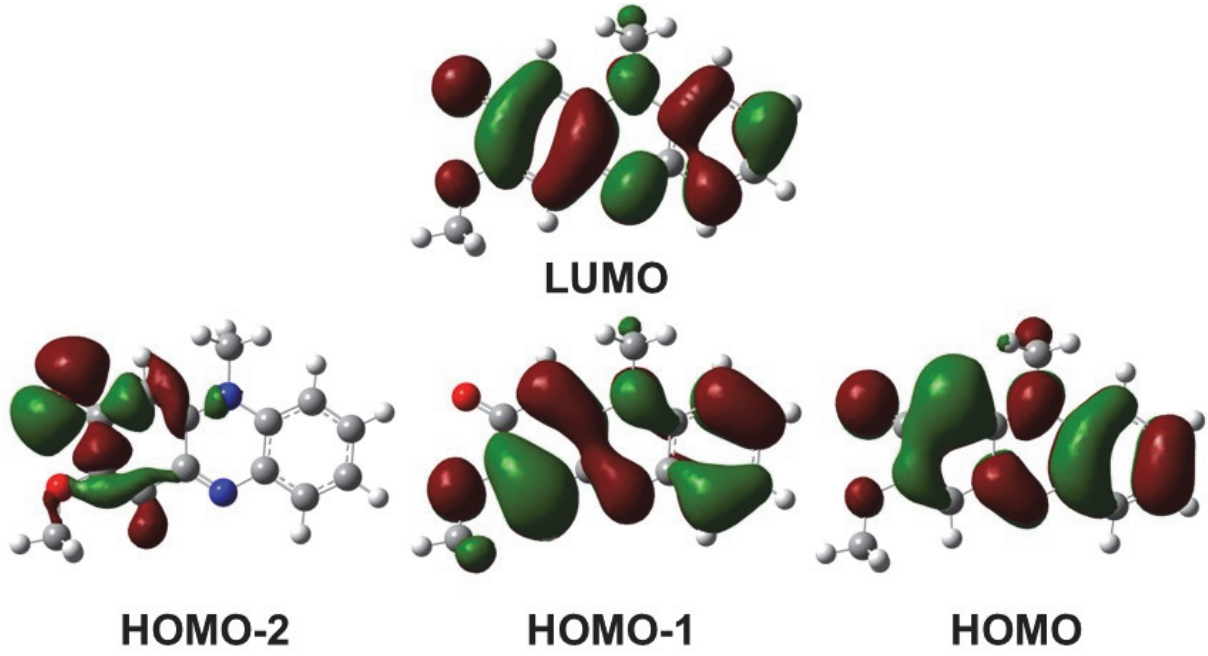

Fig. S25 Plots of visualized orbitals based on the optimized geometry of **PZ2** derived from DFT calculations at B3LYP/6-311G(d,p) level.

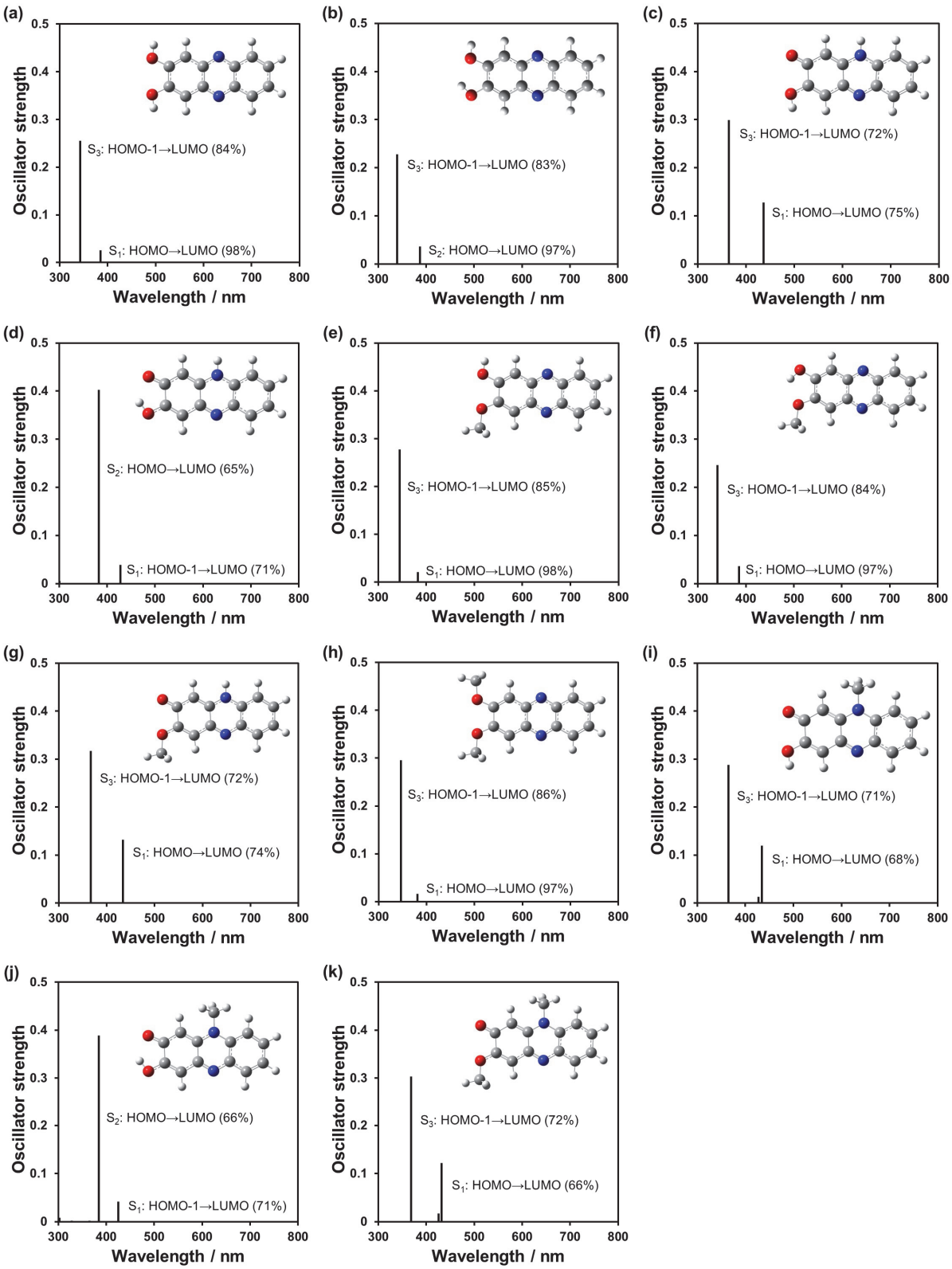

Fig. S26 Calculated photoabsorption spectra of (a) *anti*-**PD1-E**, (b) *syn*-**PD1-E**, (c) *anti*-**PD1-K**, (d) *syn*-**PD1-K**, (e) *anti*-**PD2-E**, (f) *syn*-**PD2-E**, (g) **PD2-K**, (h) **PD3**, (i) *anti*-**PZ1**, (j) *syn*-**PZ1,** and (k) **PZ2** at B3LYP/6-311G(d,p) level.

6. Photoabsorption and fluorescence measurements

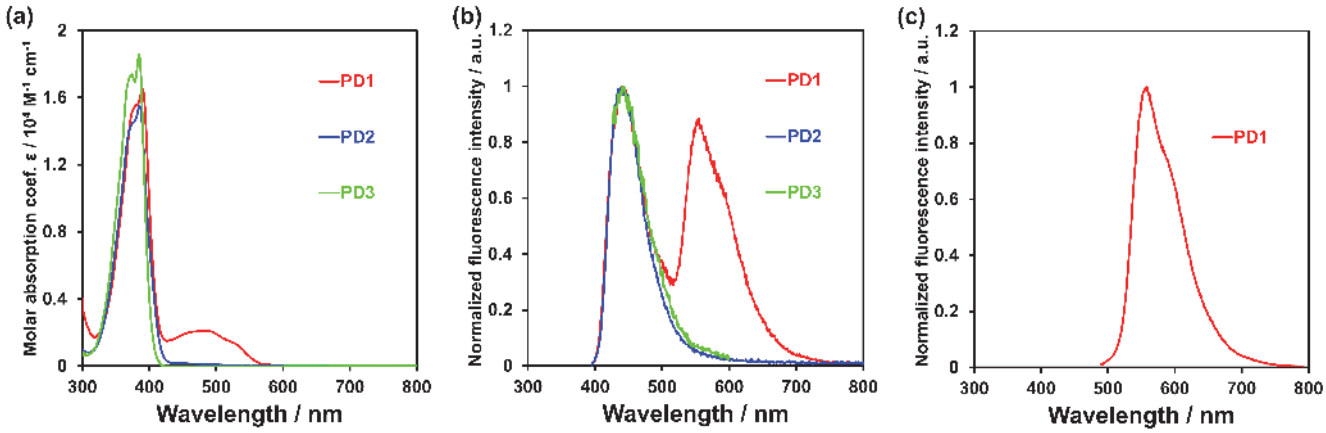

Fig. S27 (a) Photoabsorption and (b and c) normalized fluorescence (b: λ_{ex} = 385–390 nm, c: λ_{ex} = 480 nm) spectra of **PD1**–**3** (1.0×10^{-4} M) in THF.

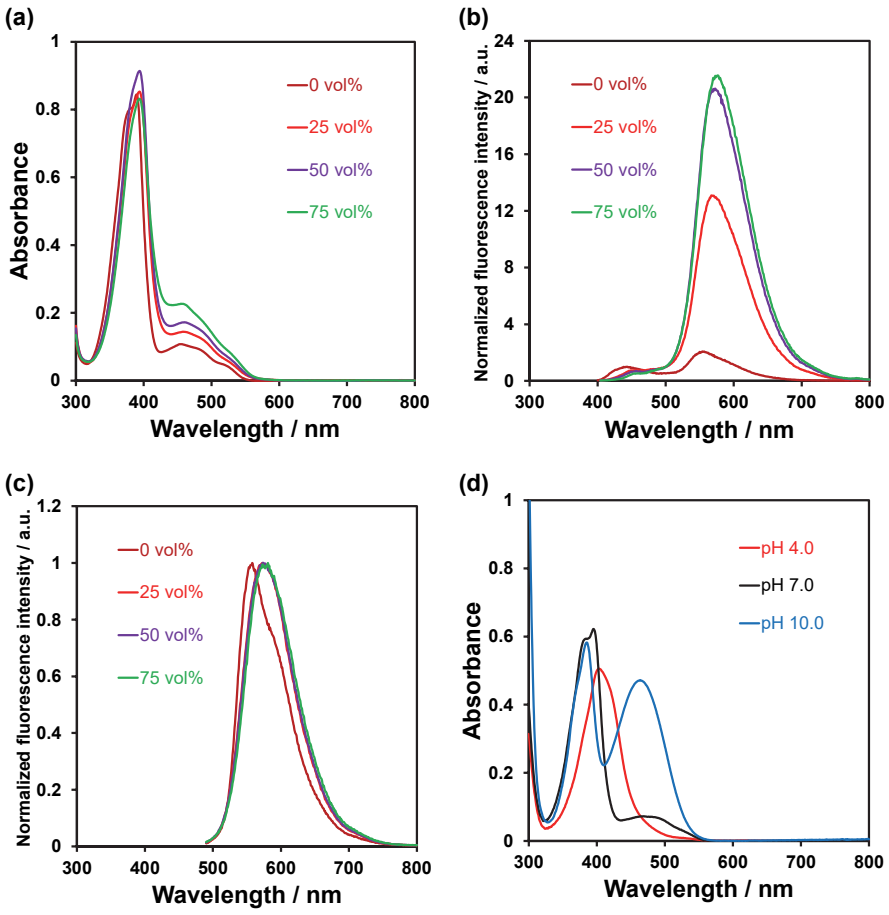

Fig. S28 (a) Photoabsorption spectra of **PD1** (5.0×10^{-5} M) in THF containing water (0–75 vol%). Normalized fluorescence (b: λ_{ex} = 390–394 nm, c: λ_{ex} = 480 nm) spectra of **PD1** (5.0×10^{-5} M) in THF containing water (0–75 vol%). (d) Photoabsorption spectra of **PD1** (5.0×10^{-5} M) in DMSO before (under pH 7) and after (pH 4 and pH 10, respectively) addition of HCl aq. and NaOH aq.

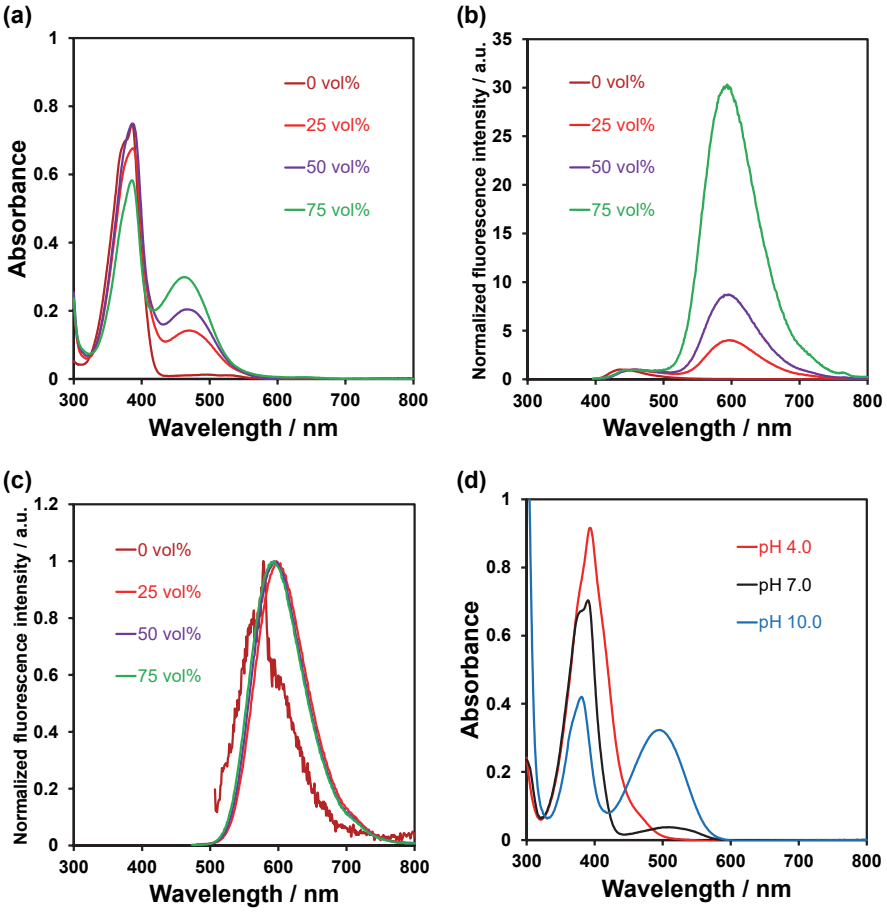

Fig. S29 (a) Photoabsorption and (b and c) normalized fluorescence (b: λ_{ex} = 386–387 nm, c: λ_{ex} = 463–497 nm) spectra of **PD2** (5.0×10^{-5} M) in THF containing water (0–75 vol%). (d) Photoabsorption spectra of **PD2** (5.0×10^{-5} M) in DMSO before (under pH 7) and after (pH 4 and pH 10, respectively) addition of HCl aq. and NaOH aq.

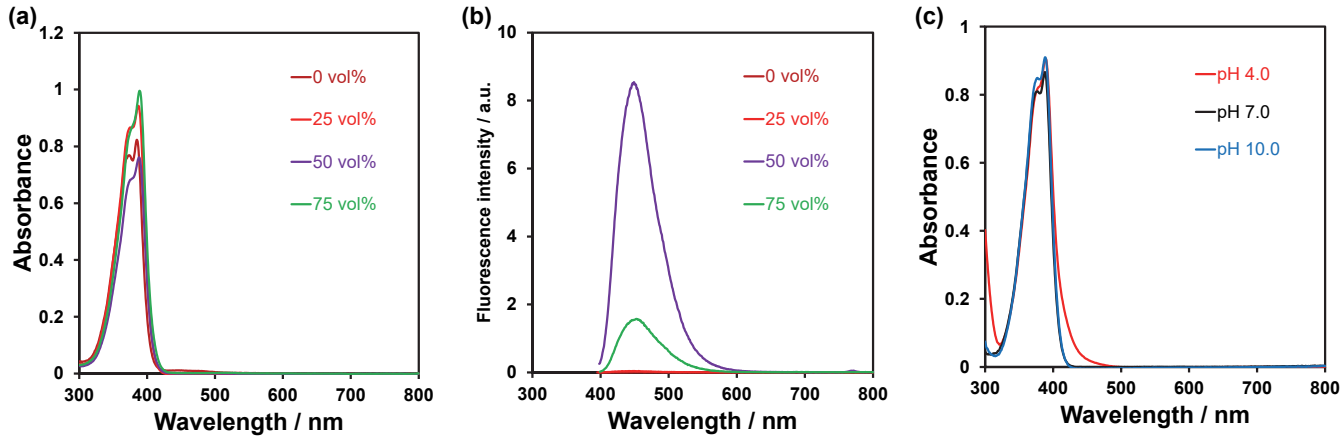

Fig. S30 (a) Photoabsorption and (b) normalized fluorescence (λ_{ex} = 385–389 nm) spectra of **PD3** (5.0×10^{-5} M) in various solvents in THF containing water (0–75 vol%). (c) Photoabsorption spectra of **PD3** (5.0×10^{-5} M) in DMSO before (under pH 7) and after (pH 4 and pH 10, respectively) addition of HCl aq. and NaOH aq.

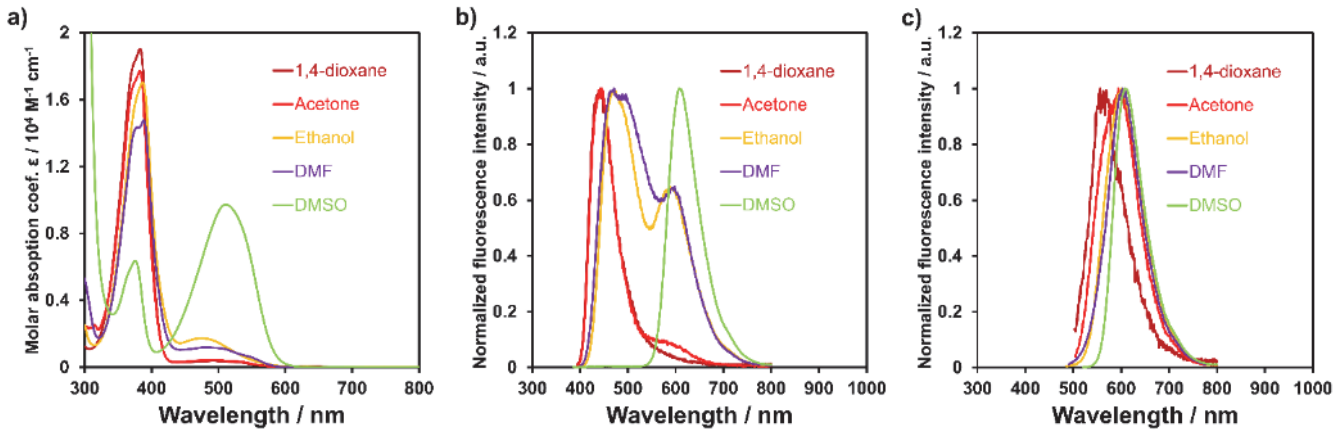

Fig. S31 (a) Photoabsorption and (b and c) normalized fluorescence (b: λ_{ex} = 378–390 nm, c: λ_{ex} = 480 nm) spectra of **PD2** (1.0×10^{-4} M) in various solvents.

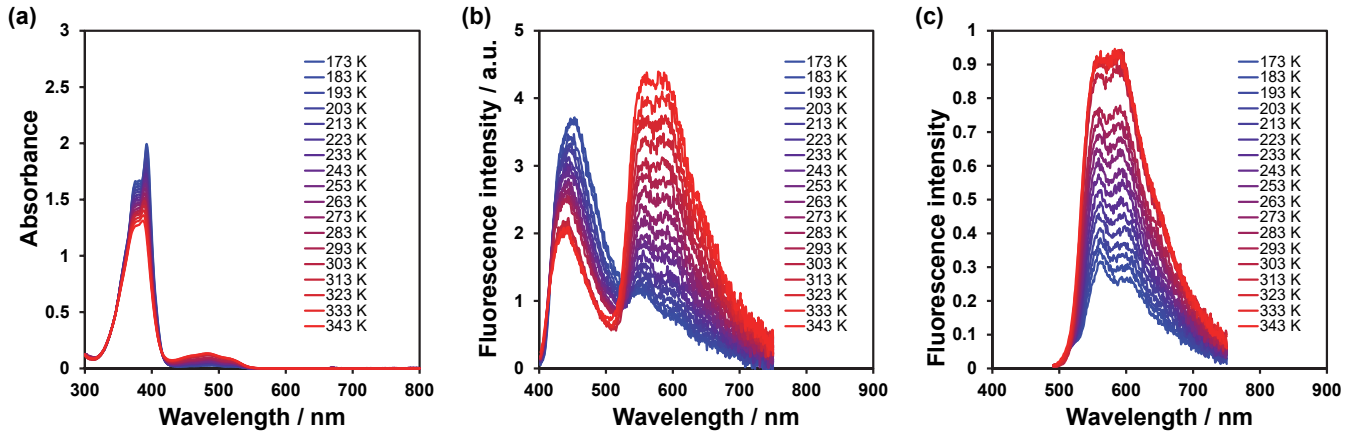

Fig. S32 Temperature-dependent (a) Photoabsorption and (b and c) fluorescence (b: λ_{ex} = 392 nm, c: λ_{ex} = 481 nm) spectra of **PD1** (1.0×10^{-4} M) from 173 K to 343 K.

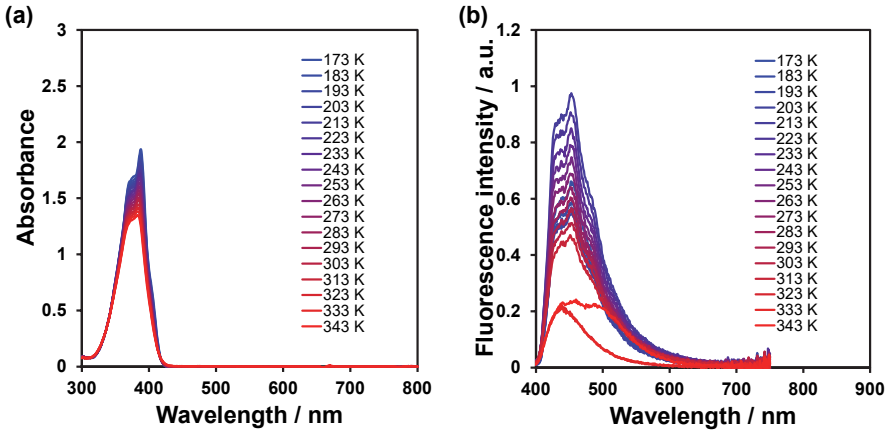

Fig. S33 Temperature-dependent (a) Photoabsorption and (b) fluorescence (λ_{ex} = 388 nm) spectra of **PD2** (1.0×10^{-4} M) from 173 K to 343 K.

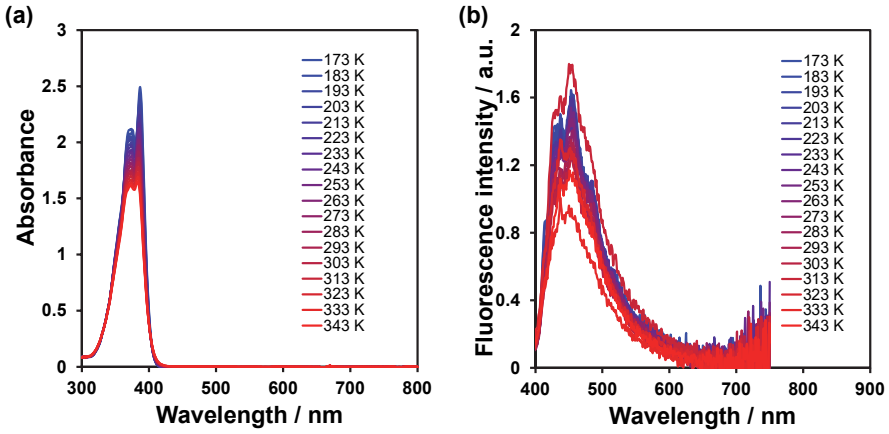

Fig. S34 Temperature-dependent (a) Photoabsorption and (b) fluorescence (λ_{ex} = 387 nm) spectra of **PD3** (1.0×10^{-4} M) from 173 K to 343 K.

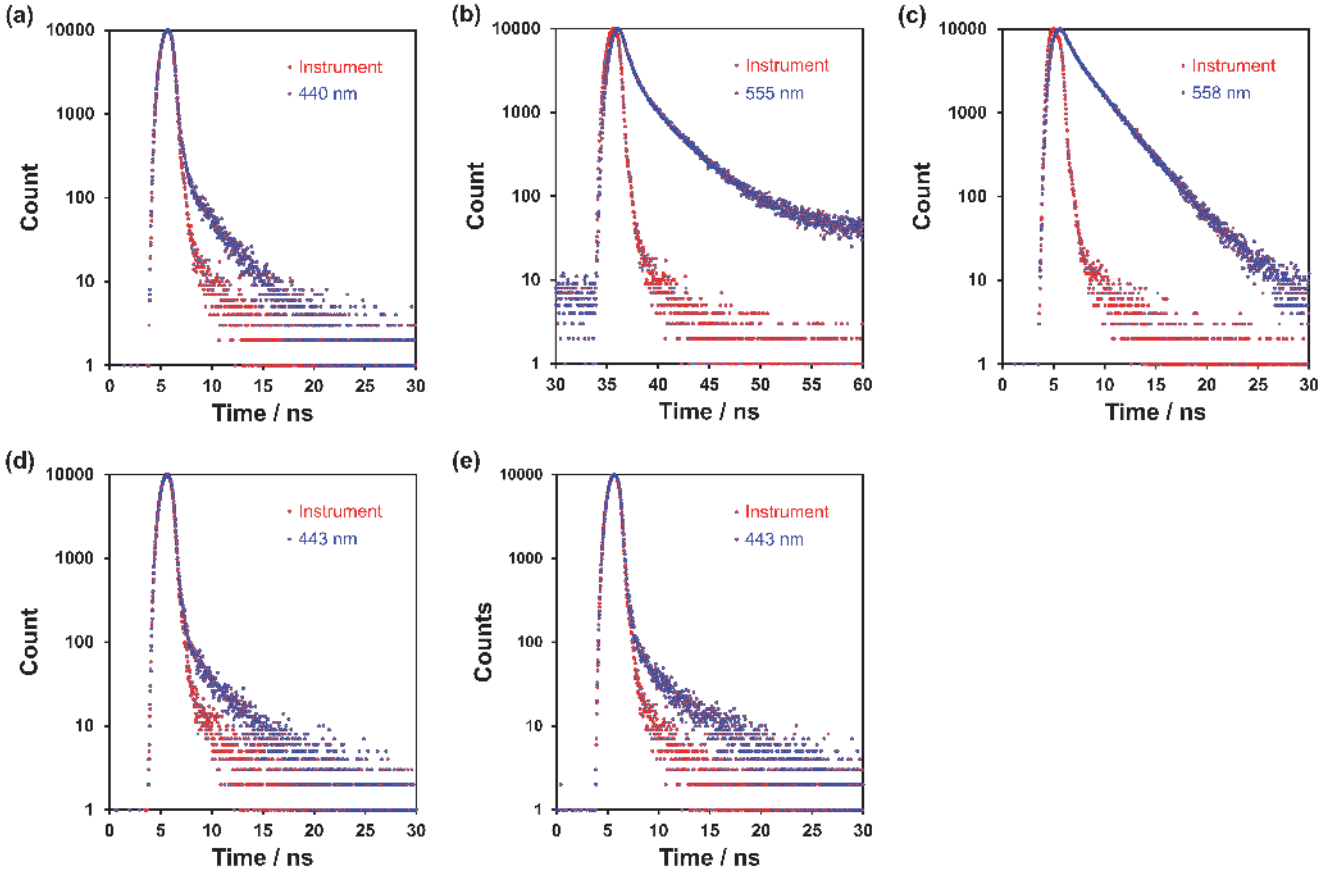

Fig. S35 Instrument profiles (red dots) and fluorescence decay profiles (blue dots) of (a, b and c) **PD1** (a: λ_{ex} = 366 nm, b: λ_{ex} = 366 nm, c: λ_{ex} = 451 nm), (d) **PD2** (λ_{ex} = 366 nm), and (e) **PD3** (λ_{ex} = 366 nm).

7. Photo-induced proton tautomerism

The photoabsorption and fluorescence spectral measurements of **PD1**–**3**, **PZ1**, and **PZ2** were performed in 2-methyltetrahydrofuran (2-MeTHF) at room temperature (298 K) and a glassy matrix of 2-MeTHF at 77 K.[S3] A 1.0 cm quartz cuvette was used in measurements at 298 K and a 0.4 cm quartz tube at 77 K. The solutions were irradiated with light-emitting diode (LED) light with a peak wavelength of 385 nm for 4 minutes (22.3 mW cm^{-2}, LDR2-100VL2-385-W, CCS). The photoabsorption and fluorescence spectra of these solutions were measured immediately after photoirradiation.

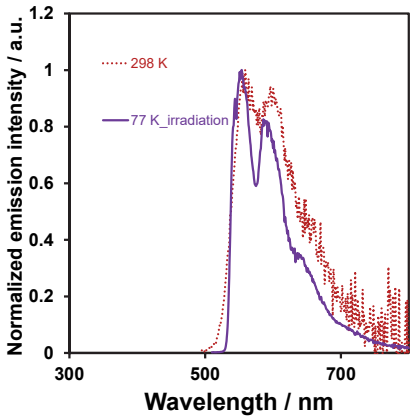

Fig. S36 Normalized fluorescence (λ_{ex} = 485–500 nm) spectra of **PD1** in 2-MeTHF at 298 (dashed line) and 77 K (solid lines) after irradiation with monochromic light at 385 nm.

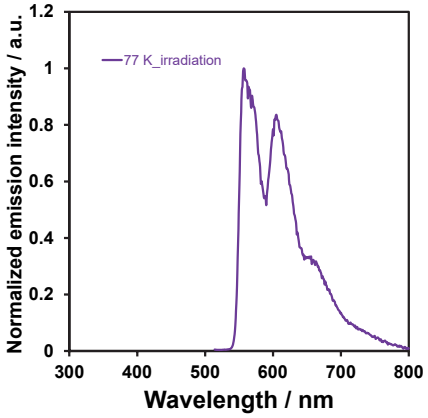

Fig. S37 Normalized fluorescence (λ_{ex} = 504 nm) spectra of **PD2** in 2-MeTHF at 77 K after irradiation with monochromic light at 385 nm.

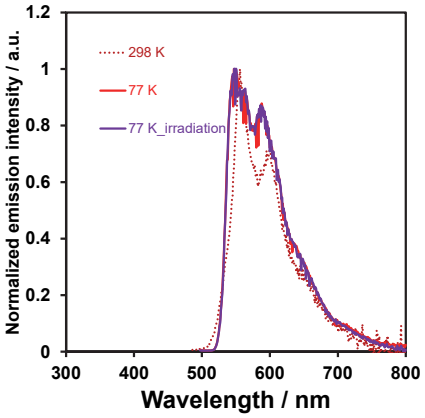

Fig. S38 Normalized fluorescence (λ_{ex} = 476–487 nm) spectra of **PZ1** in 2-MeTHF at 298 (dashed line) and 77 K (solid lines) before and after irradiation with monochromic light at 385 nm.

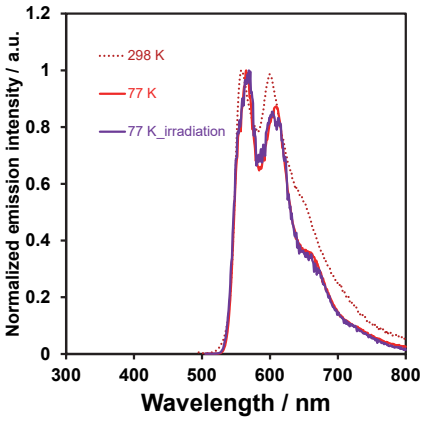

Fig. S39 Normalized fluorescence (λ_{ex} = 485–495 nm) spectra of **PZ2** in 2-MeTHF at 298 (dashed line) and 77 K (solid lines) before and after irradiation with monochromic light at 385 nm.

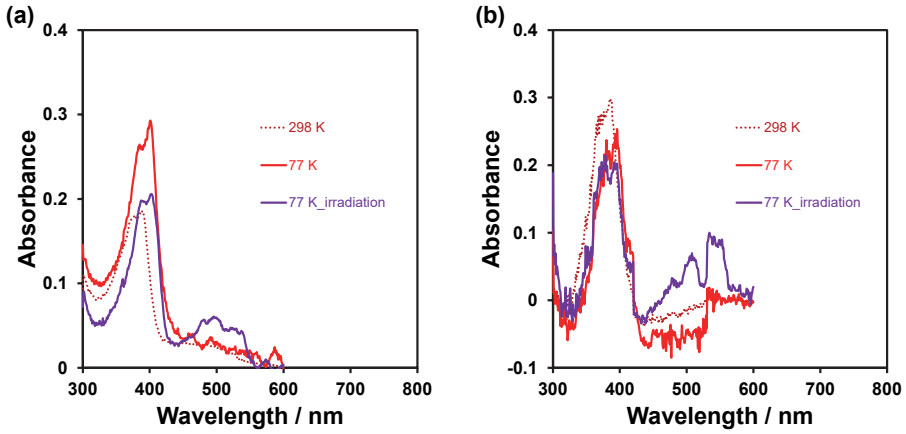

Fig. S40 Photoabsorption spectra of (a) **PD1** and (b) **PD2** in 2-MeTHF (10 μM) at 298 K (dashed line) and 77 K (solid line) before and after irradiation with monochromic light at 385 nm.

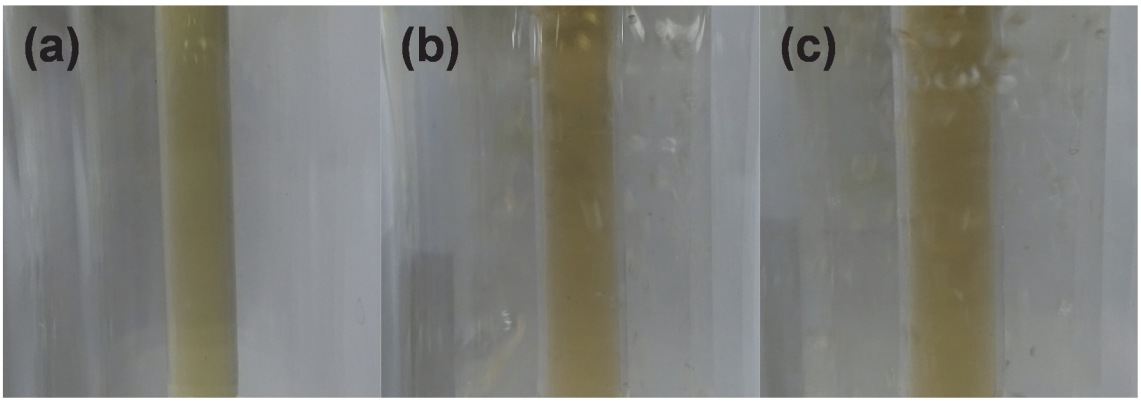

Fig. S41 Photographs of **PZ1** in 2-MeTHF (a: 298 K, b: 77 K, and c: 77 K after photoirradiation at 385 nm).

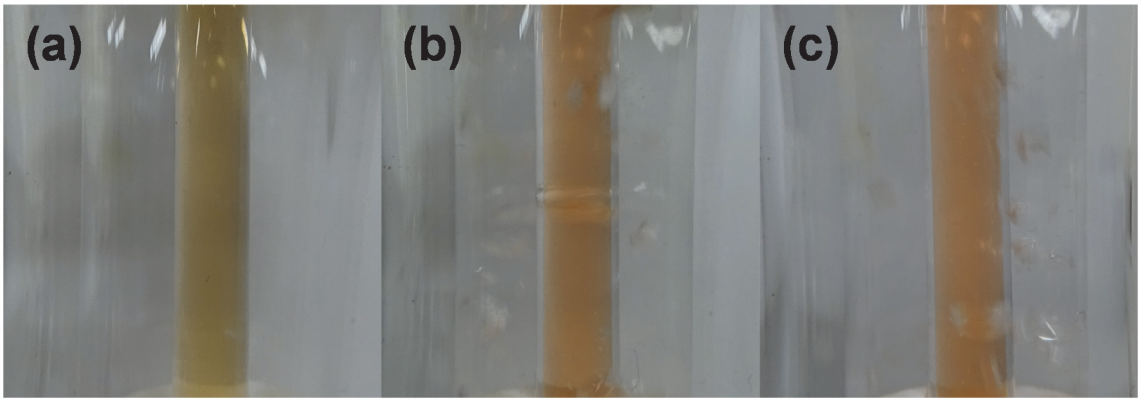

Fig. S42 Photographs of **PZ2** in 2-MeTHF (a: 298 K, b: 77 K, and c: 77 K after photoirradiation at 385 nm).

8. Phosphorescence measurements

In order to assign the emission bands of **PD3** that appeared in the range of 600-800 nm in 2-MeTHF at 77K (Fig. 6f), phosphorescence measurements were performed for **PD1**–**3**, **PZ1**, and **PZ2**, with an initial delay of 100 μs.

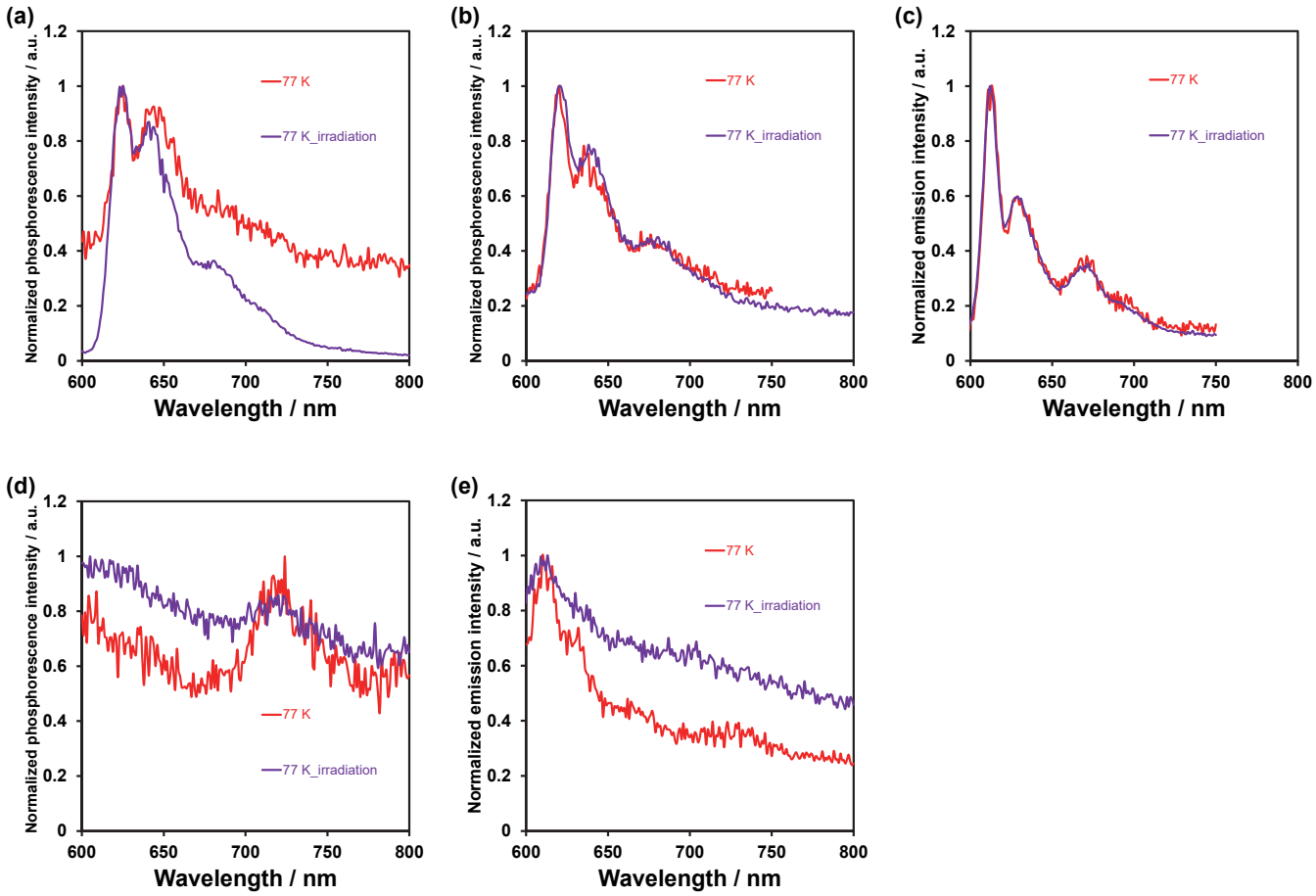

Fig. S43 Phosphorescence spectra of (a) **PD1** (λ_{ex} = 400 nm), (b) **PD2** (λ_{ex} = 395 nm), (c) **PD3** (λ_{ex} = 385 nm), (d) **PZ1** (λ_{ex} = 397 nm), and (e) **PZ2** (λ_{ex} = 370 nm) in 2-MeTHF at 77 K before and after irradiation with monochromic light at 385 nm.

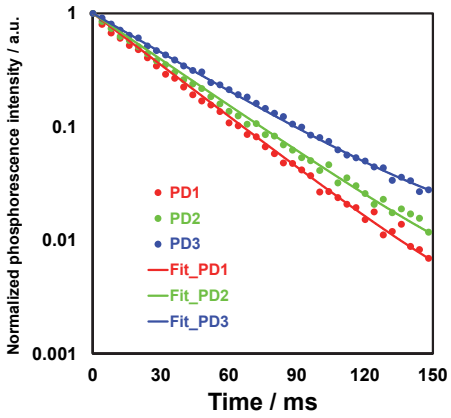

Fig. S44 Phosphorescence lifetime decay curves of **PD1** at 623 nm, **PD2** at 621 nm, and **PD3** at 612 nm in 2-MeTHF at 77K. The phosphorescence lifetimes were determined to be 28.6 ms for **PD1**, 32.0 ms for **PD2**, and 37.3 ms for **PD3**.

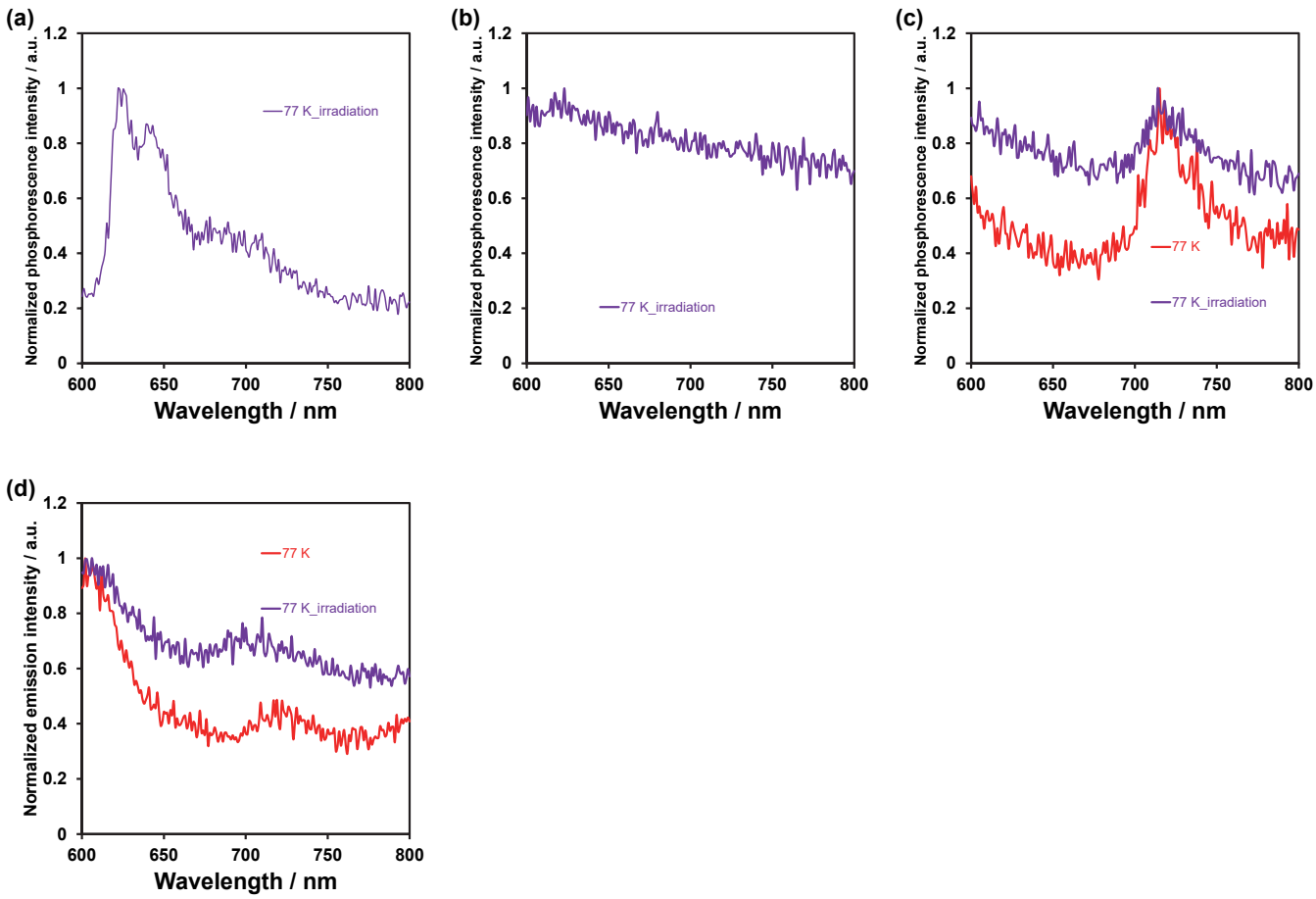

Fig. S45 Phosphorescence spectra of (a) **PD1** (λ_{ex} = 500 nm), (b) **PD2** (λ_{ex} = 504 nm), (c) **PZ1** (λ_{ex} = 487 nm), and (d) **PZ2** (λ_{ex} = 495 nm) in 2-MeTHF at 77 K after irradiation with monochromic light at 385 nm.

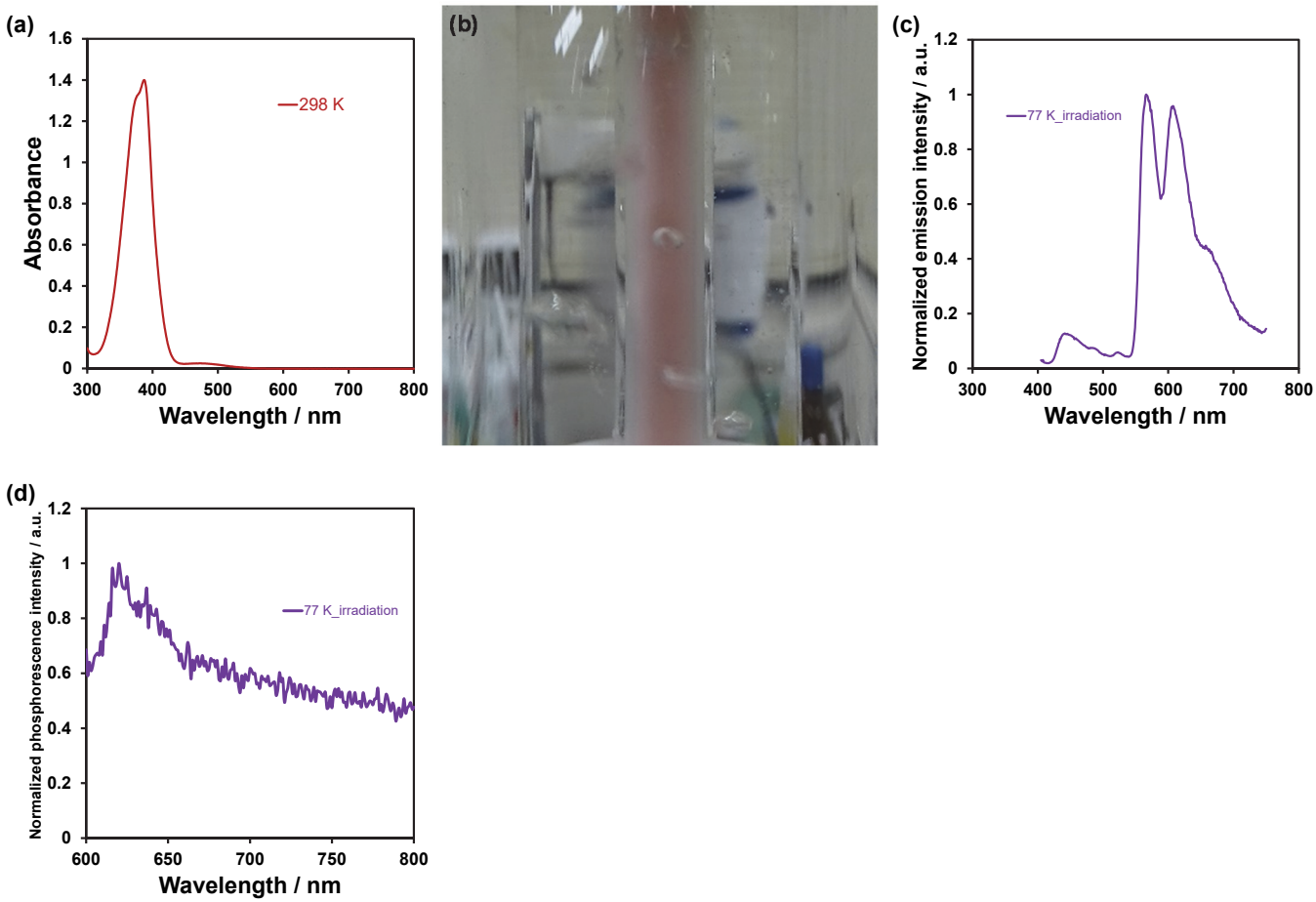

Fig. S46 (a) Photoabsorption spectrum of **PD2** (1.0×10^{-4} M) in 2-MeTHF containing water at 298 K, (b) photograph of **PD2**, (c) photoluminescence spectrum of **PD2** (λ_{ex} = 504 nm), and (d) Phosphorescence spectra of **PD2** in 2-MeTHF containing water at 77 K after irradiation with monochromic light at 385 nm.

9. Solid-state optical properties

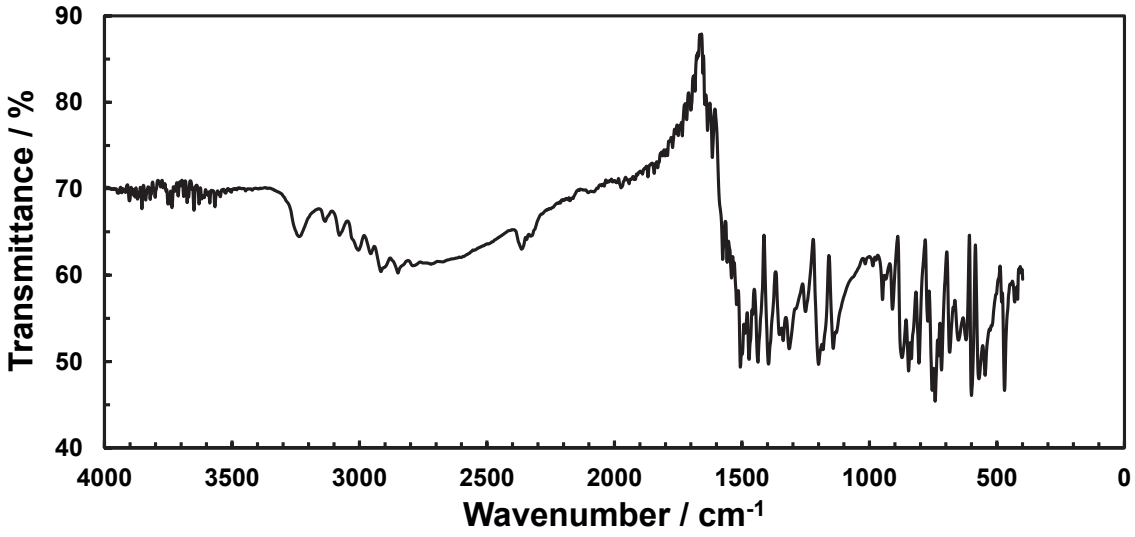

Fig. S47 ATR-FT-IR spectrum of **PD1** crystal obtained by sublimation.

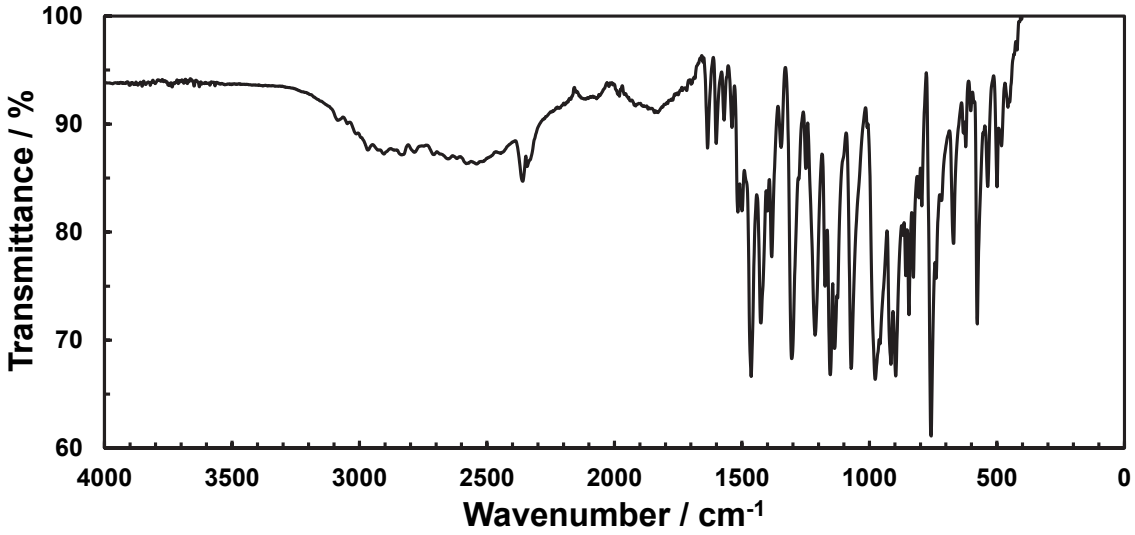

Fig. S48 ATR-FT-IR spectrum of **PD2** crystal obtained by recrystallization from an ethanol solvent.

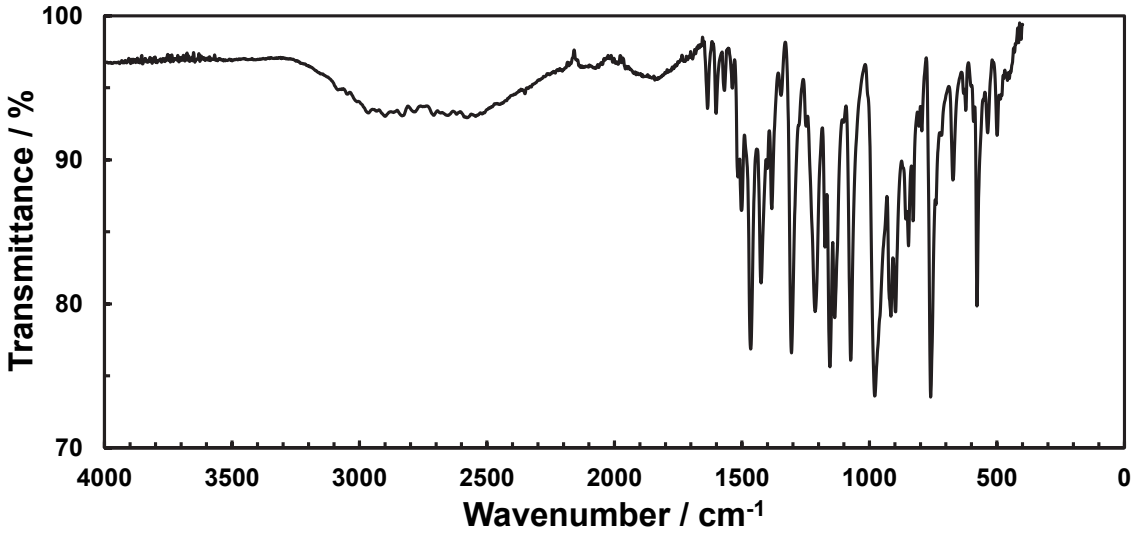

Fig. S49 ATR-FT-IR spectrum of **PD2** after heating at 133 ℃ under a pressure of 6.7×10^{-2} Pa.

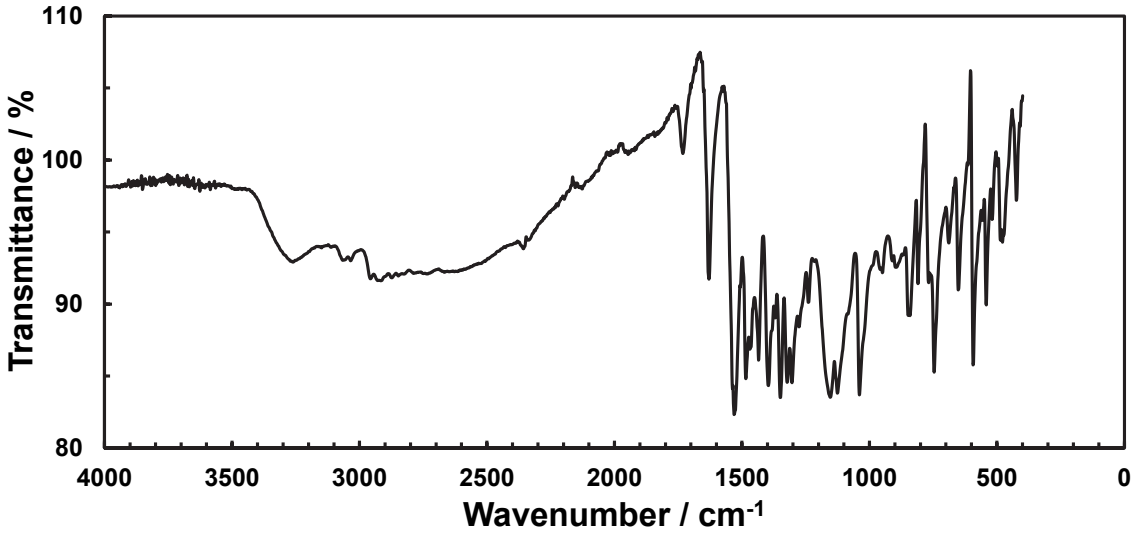

Fig. S50 ATR-FT-IR spectrum of **PD2** after heating at 205 ℃ under nitrogen atmosphere.

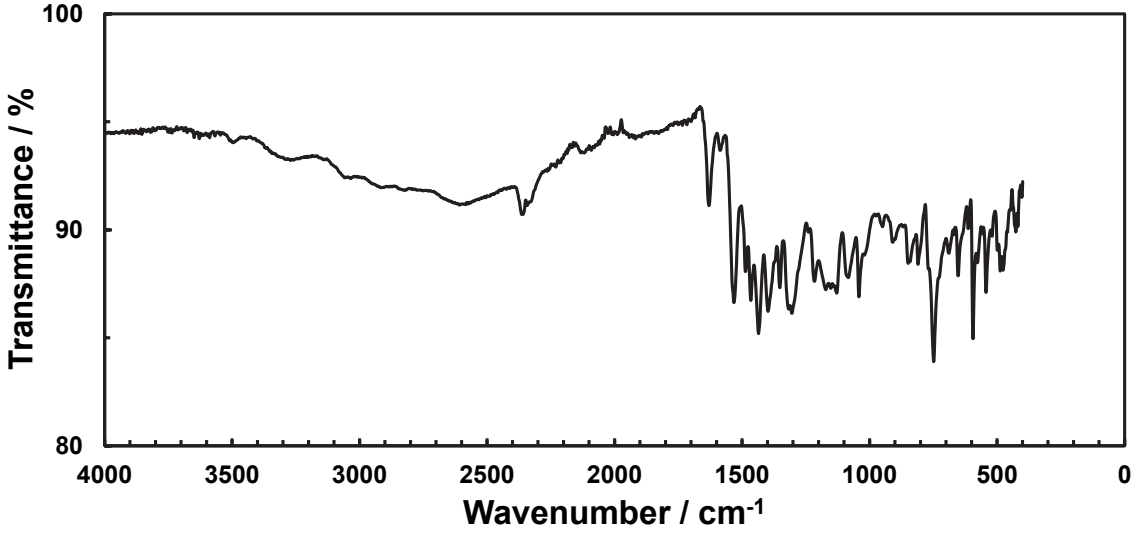

Fig. S51 ATR-FT-IR spectrum of **PD2** after heating at 270 ℃ under nitrogen atmosphere.

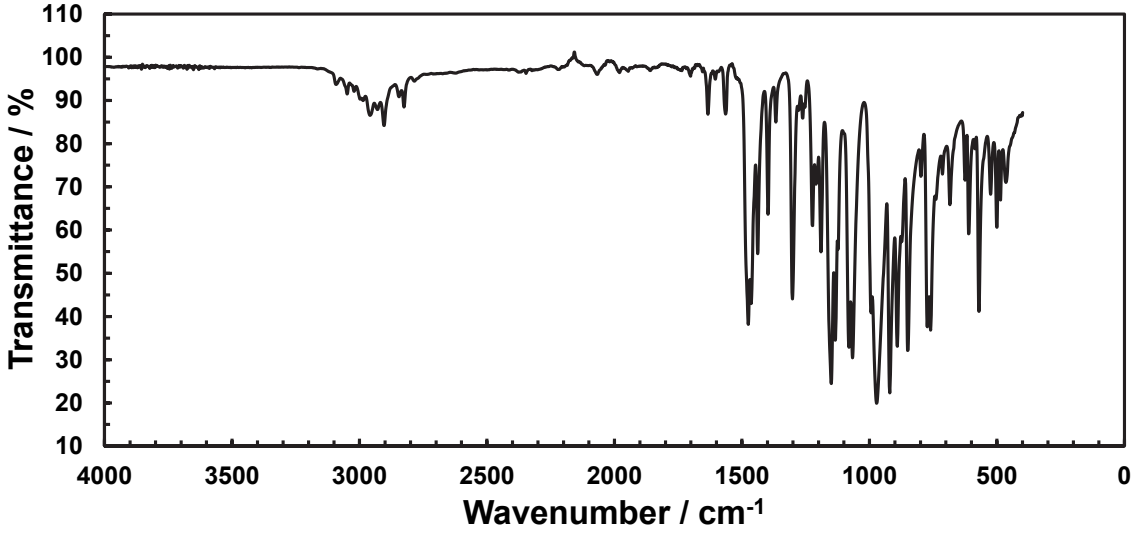

Fig. S52 ATR-FT-IR spectrum of **PD3** powder obtained by reprecipitation from a mixed solvent of THF/hexane.

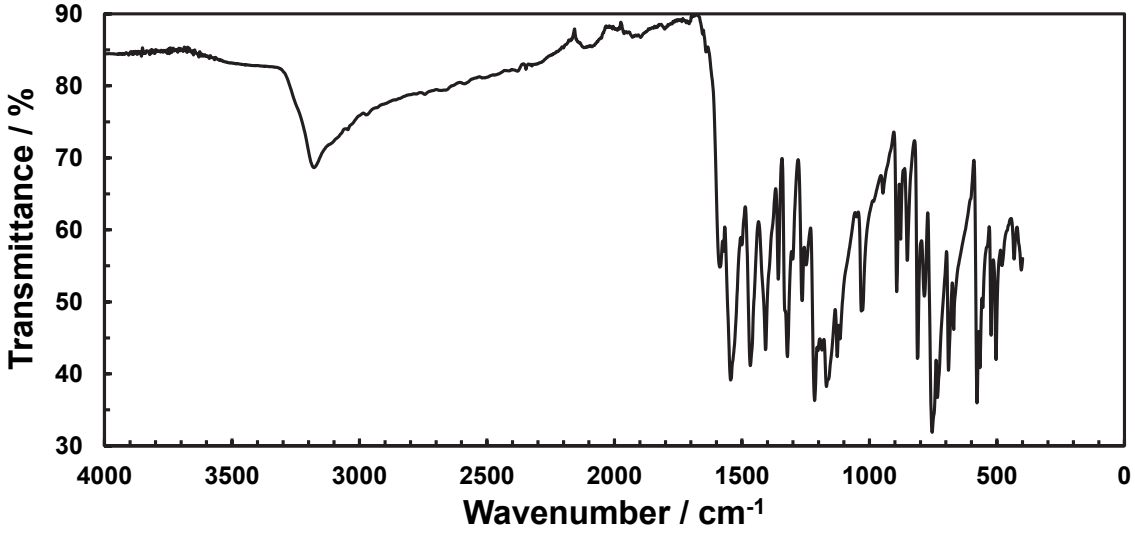

Fig. S53 ATR-FT-IR spectrum of **PZ1** crystal obtained by recrystallization from a mixed solvent of CH_2Cl_2/hexane.[S1]

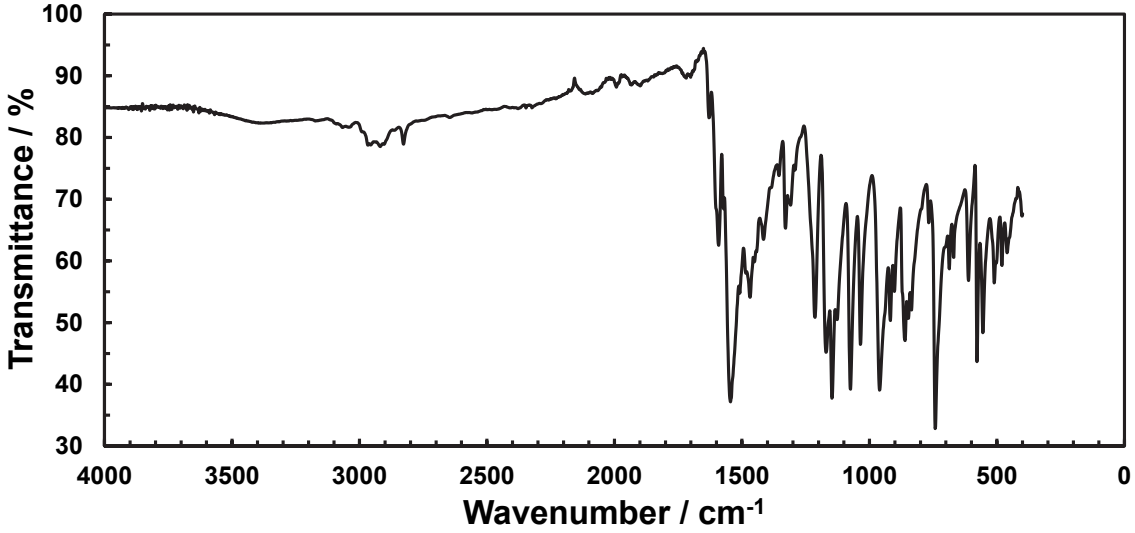

Fig. S54 ATR-FT-IR spectrum of **PZ2** crystal obtained by recrystallization from a mixed solvent of CH_2Cl_2/hexane.[S1]

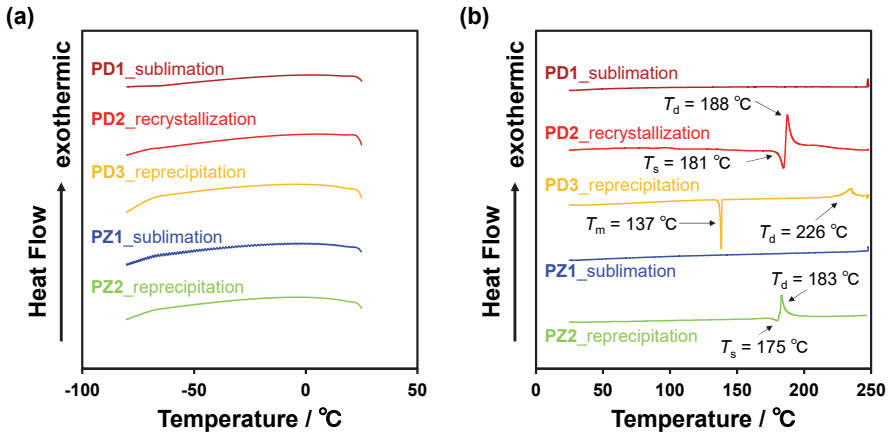

Fig. S55 DSC curves (a: cooling process from 25 ℃ to −80 ℃ with a scan rate of 10 ℃ min^{-1} and b: heating process from 25 ℃ to 250 ℃ with a scan rate of 1 ℃ min^{-1}) of **PD1**–**3**, **PZ1**, and **PZ2**.

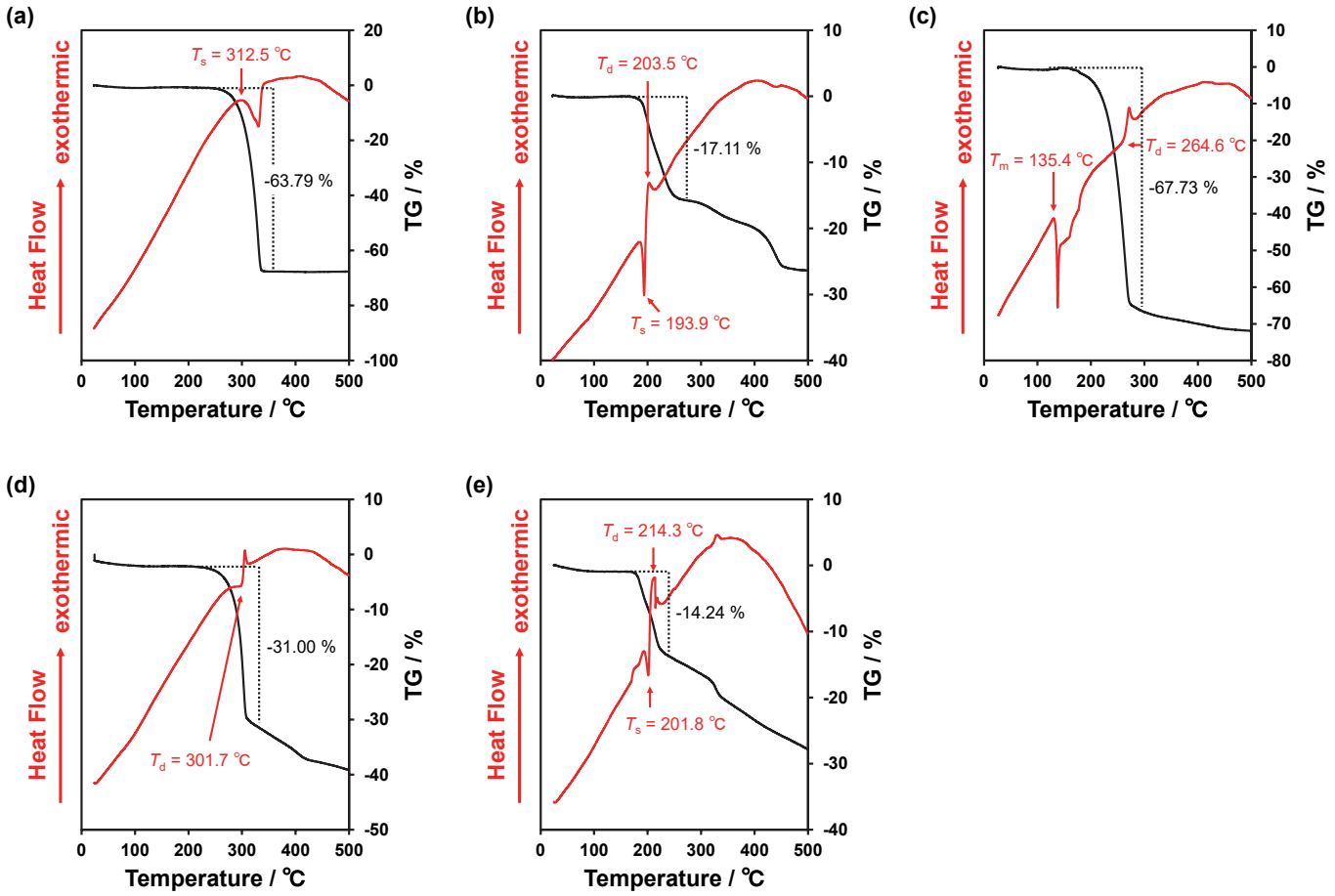

Fig. S56 DTA-TG curves (heating process from 25 ℃ to 500 ℃ with a scan rate of 10 ℃ min^{-1}) of (a) **PD1**, (b) **PD2**, (c) **PD3**, (d) **PZ1**, and (e) **PZ2**. Temperatures at 5% weight loss ($T_{5\%}$) are 285 ℃ for **PD1**, 203 ℃ for **PD2**, 209 ℃ for **PD3**, 272 ℃ for **PZ1**, and 194 ℃ for **PZ2**.

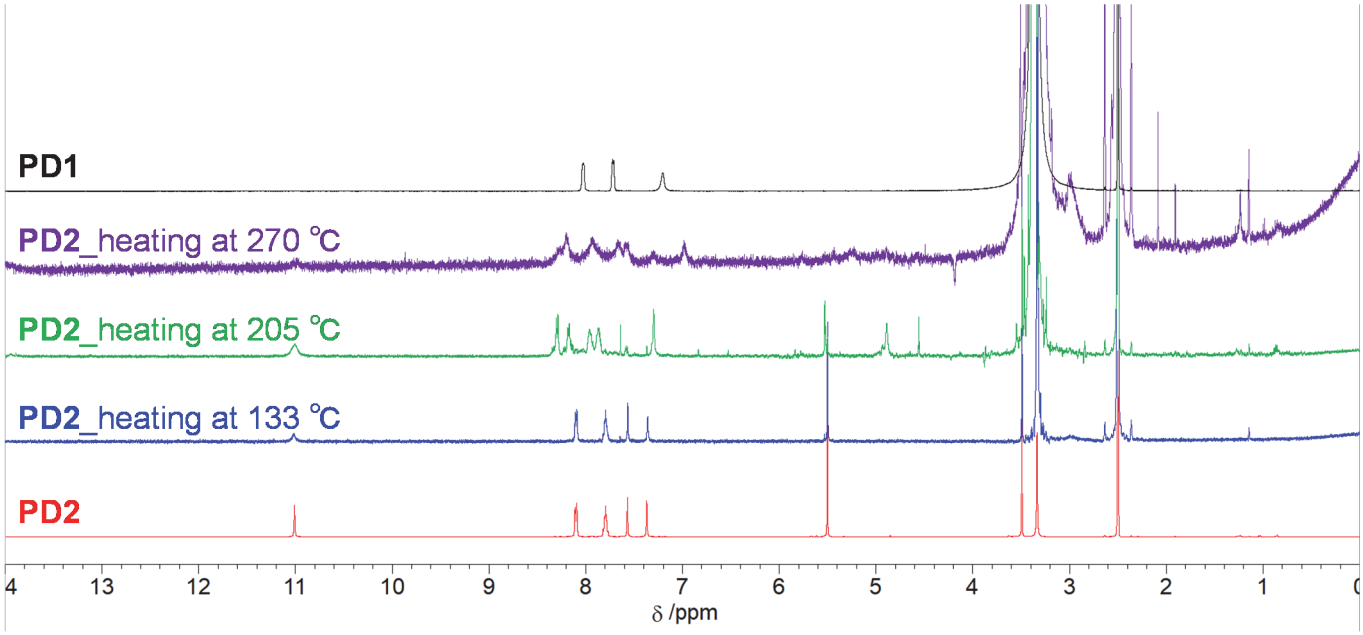

Fig. S57 ^{1}H NMR spectra of **PD2**, **PD2** after heating at 133 ℃ under vacuum, **PD2** after heating at 205 ℃, **PD2** after heating at 270 ℃ under nitrogen atmosphere, and **PD1** in DMSO-d_6.

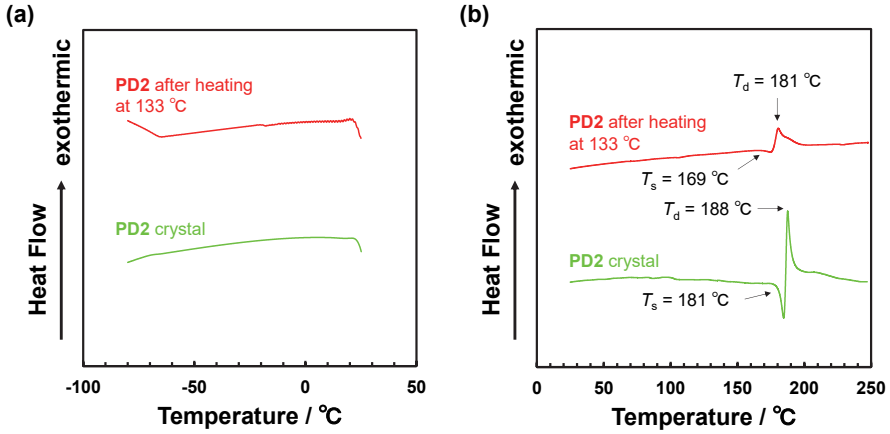

Fig. S58 DSC curves (a: cooling process from 25 ℃ to −80 ℃ with a scan rate of 10 ℃ min^{-1} and b: heating process from 25 ℃ to 250 ℃ with a scan rate of 1 ℃ min^{-1}) of solid of sublimate obtained by heating the crystals of **PD2** at 133 °C under vacuum (red) and crystals of **PD2** obtained by the recrystallization from the ethanol solution (green).

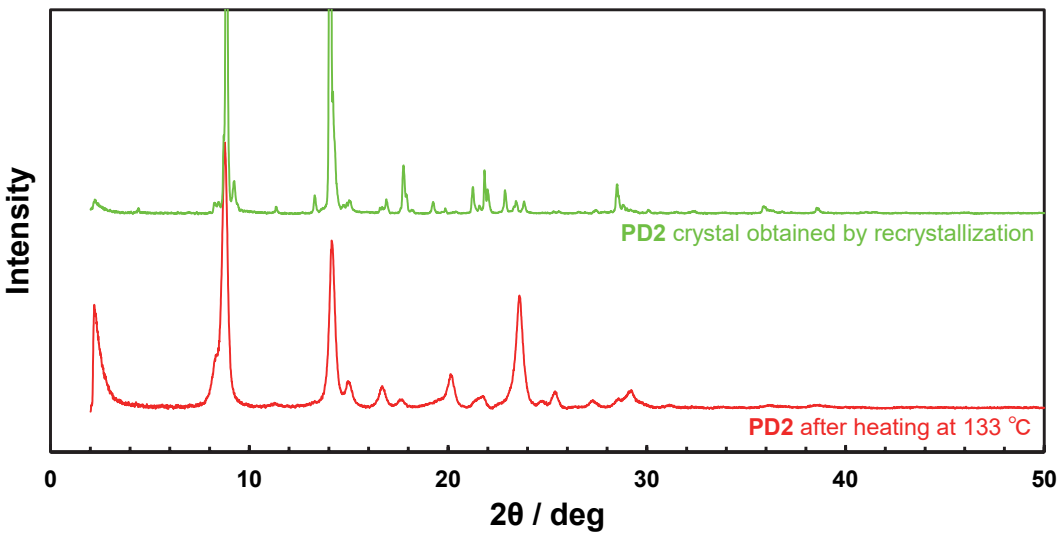

Fig. S59 Powder X-ray diffraction patterns of crysta1s of **PD2** obtained by the recrystallization from the ethanol solution (green) and solid of sublimate obtained by heating the crystals of **PD2** at 133 °C under vacuum (red).

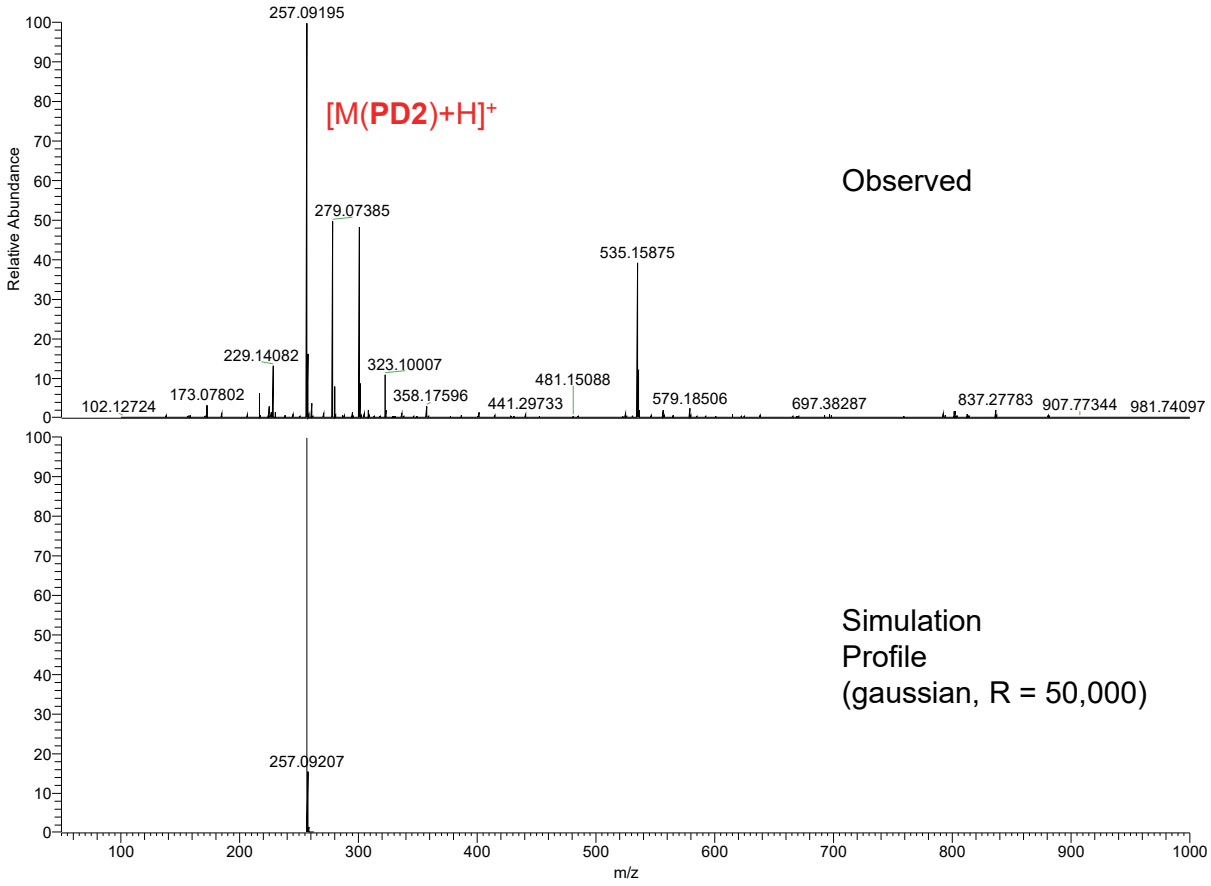

Fig. S60 HRMS spectrum (ESI, positive) of **PD2**.

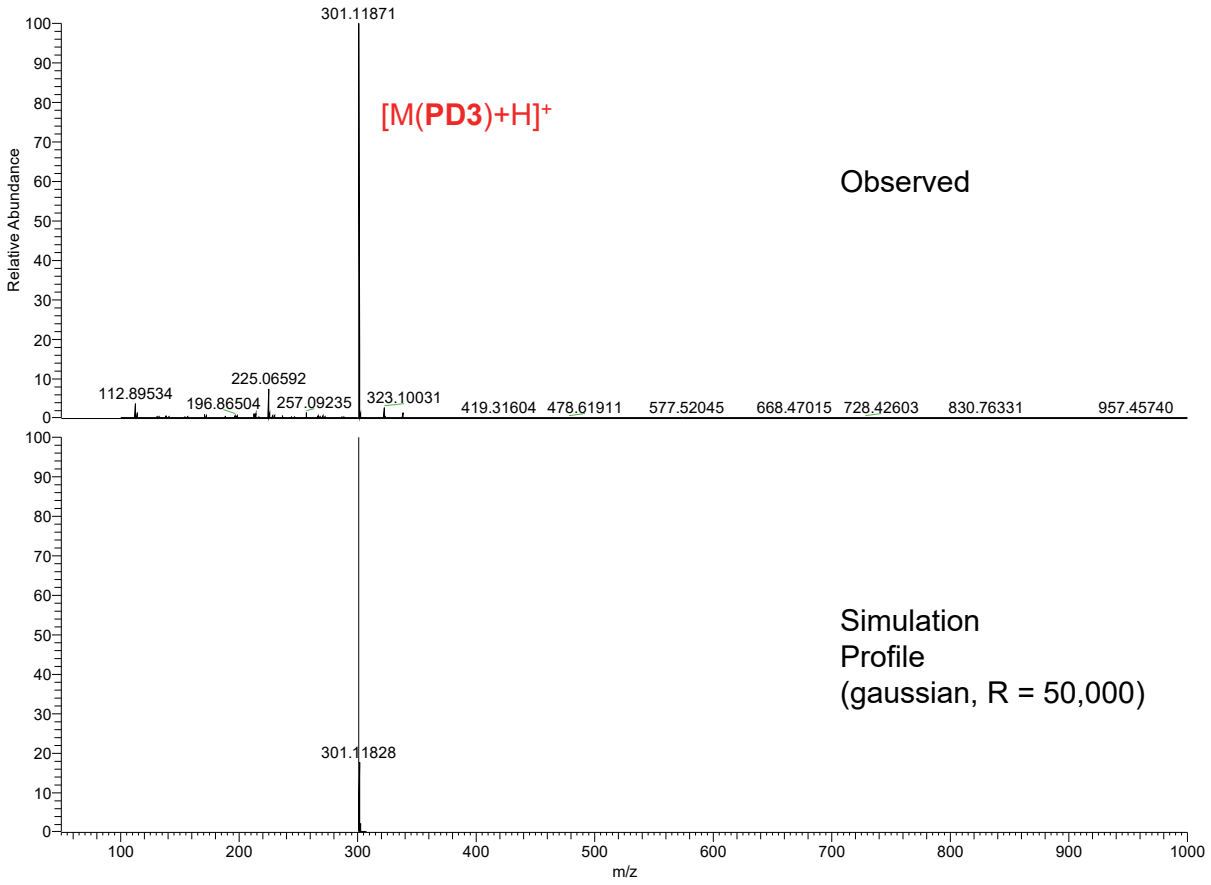

Fig. S61 HRMS spectrum (APCI, positive) of **PD3**.

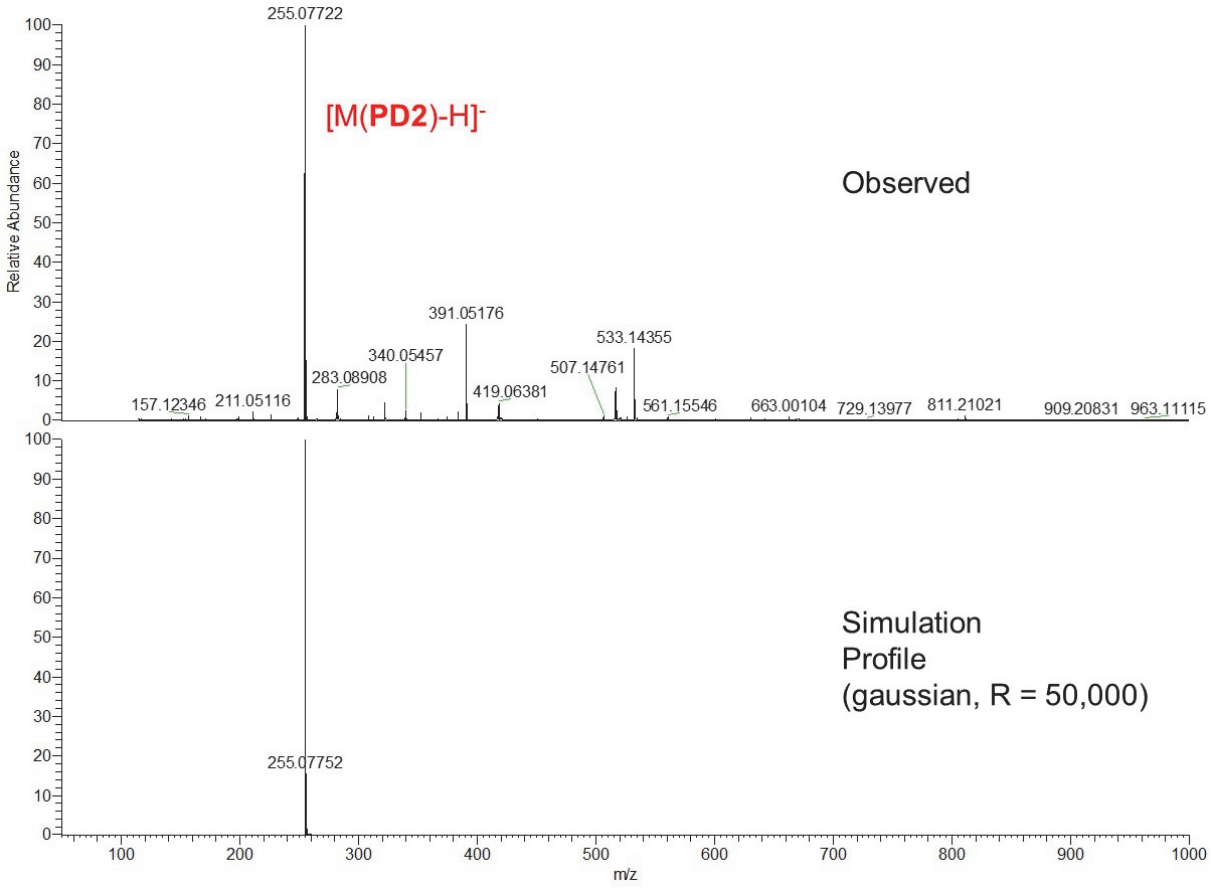

Fig. S62 HRMS spectrum (ESI, negative) of **PD2** after heating at 133 °C under vacuum.

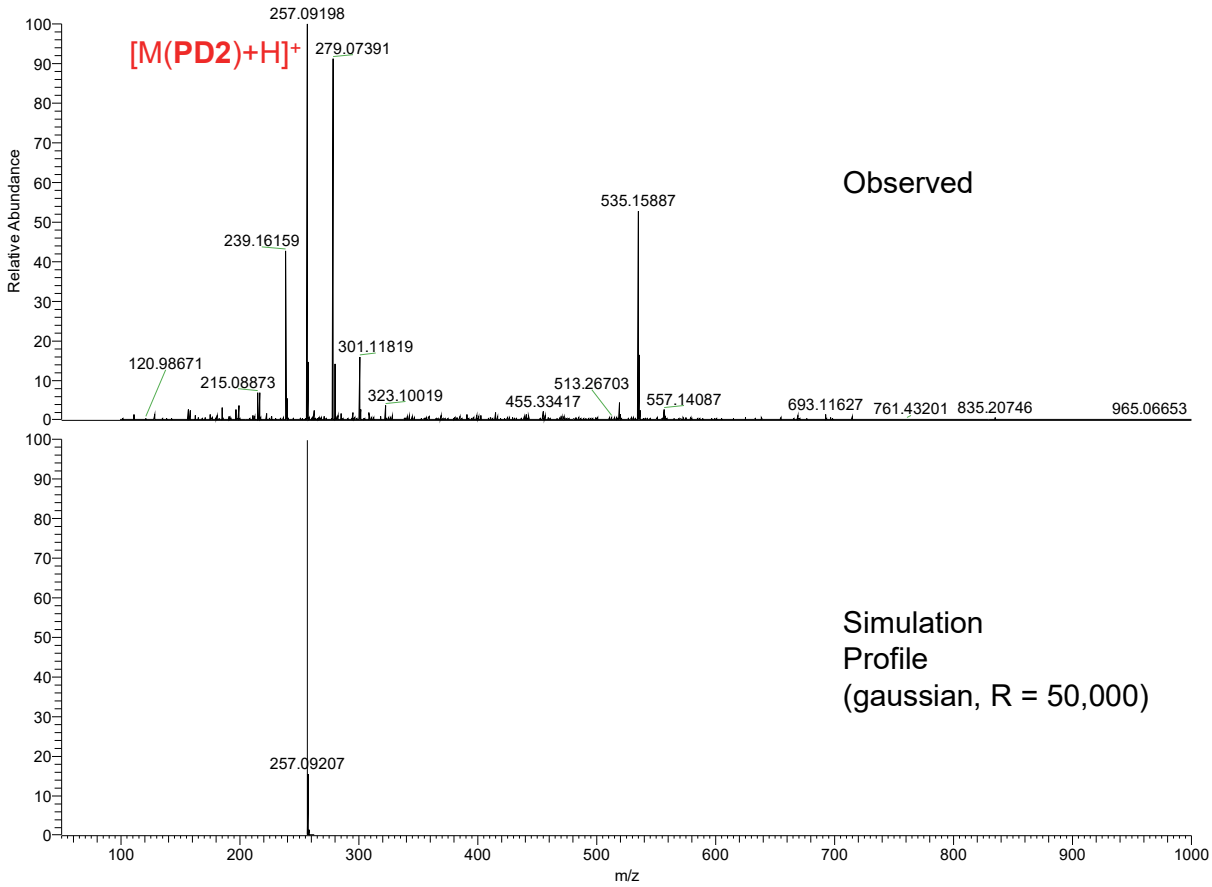

Fig. S63 HRMS spectrum (ESI, positive) of **PD2** after heating at 133 °C under vacuum.

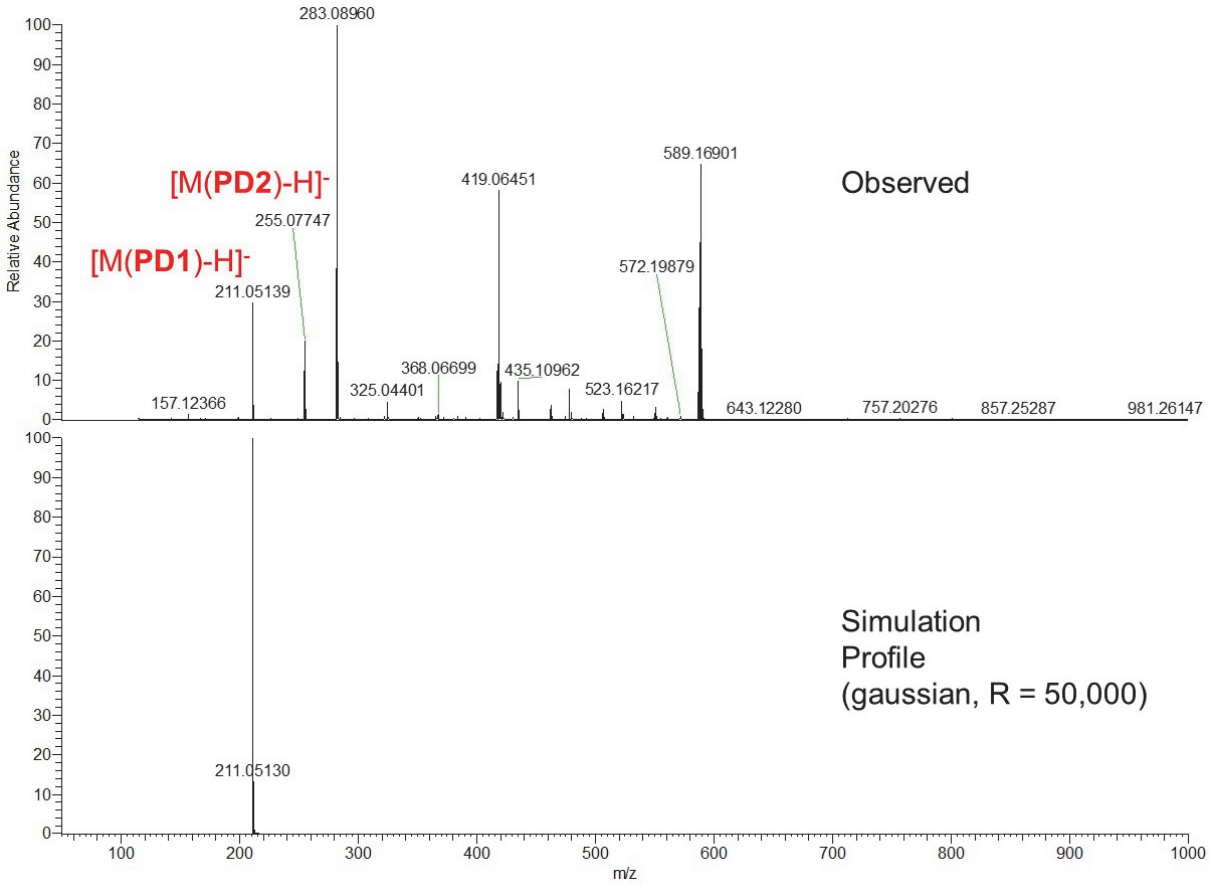

Fig. S64 HRMS spectrum (ESI, negative) of **PD2** after heating at 205 °C under nitrogen atmosphere.

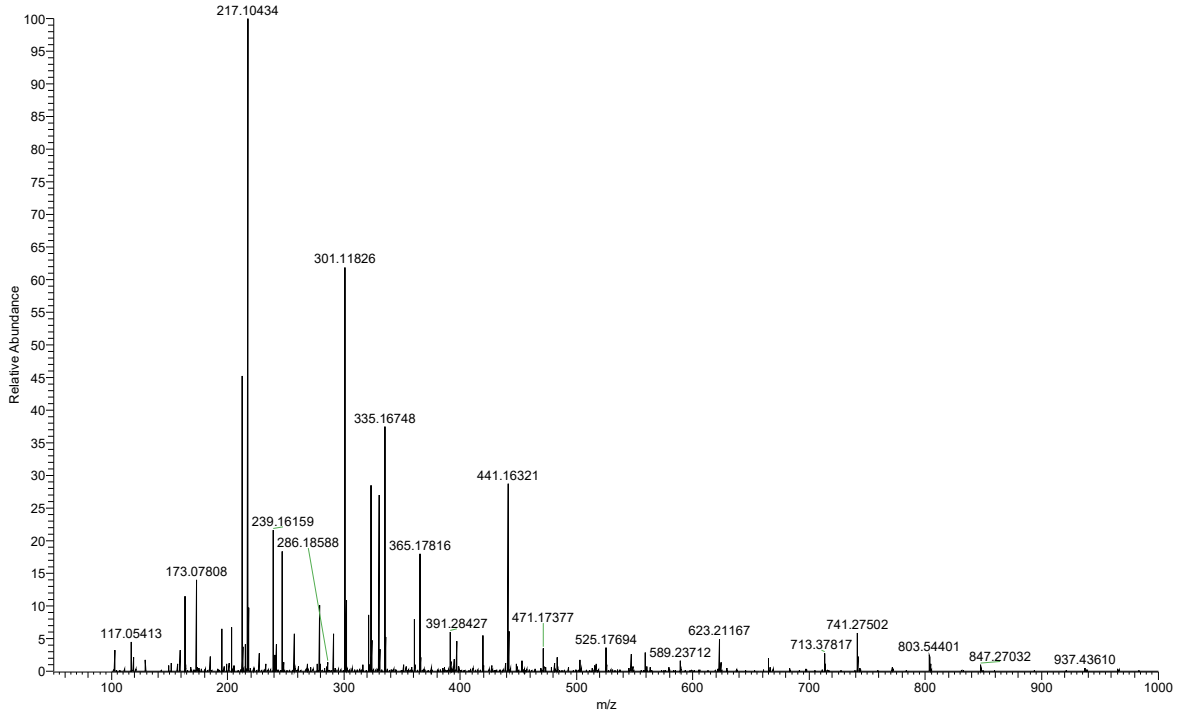

Fig. S65 HRMS spectrum (ESI, positive) of **PD2** after heating at 205 °C under nitrogen atmosphere.

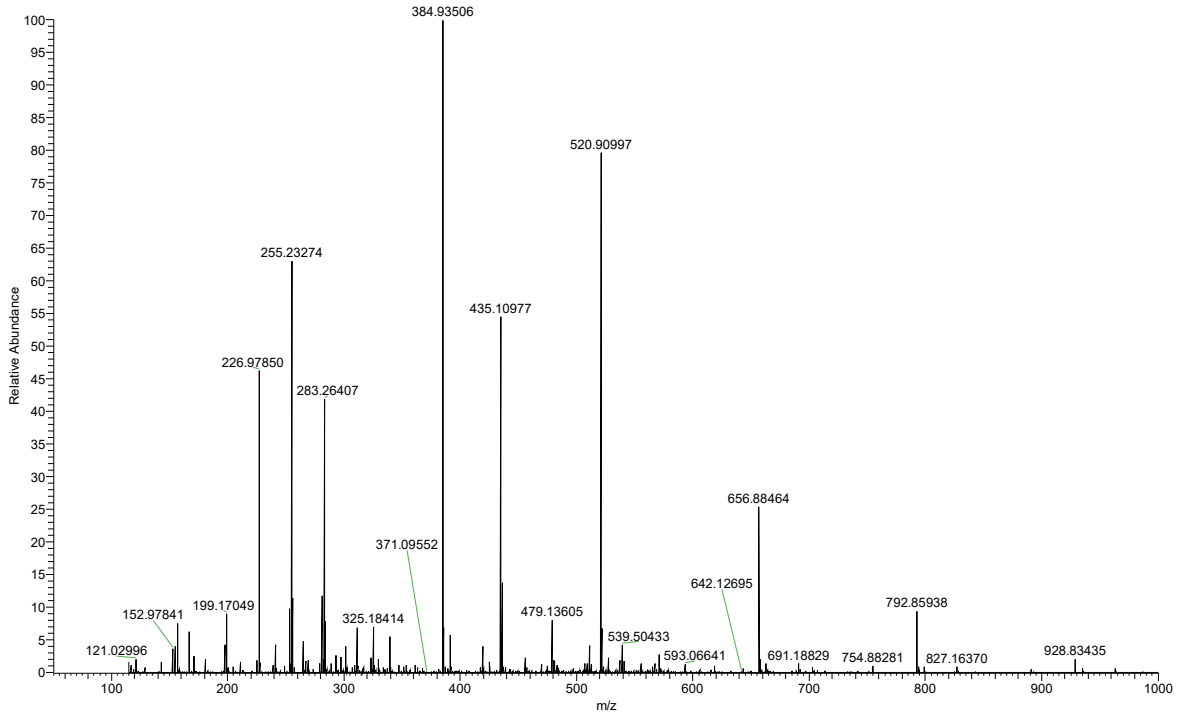

Fig. S66 HRMS spectrum (ESI, negative) of **PD2** heating at 270 ℃ under nitrogen atmosphere.

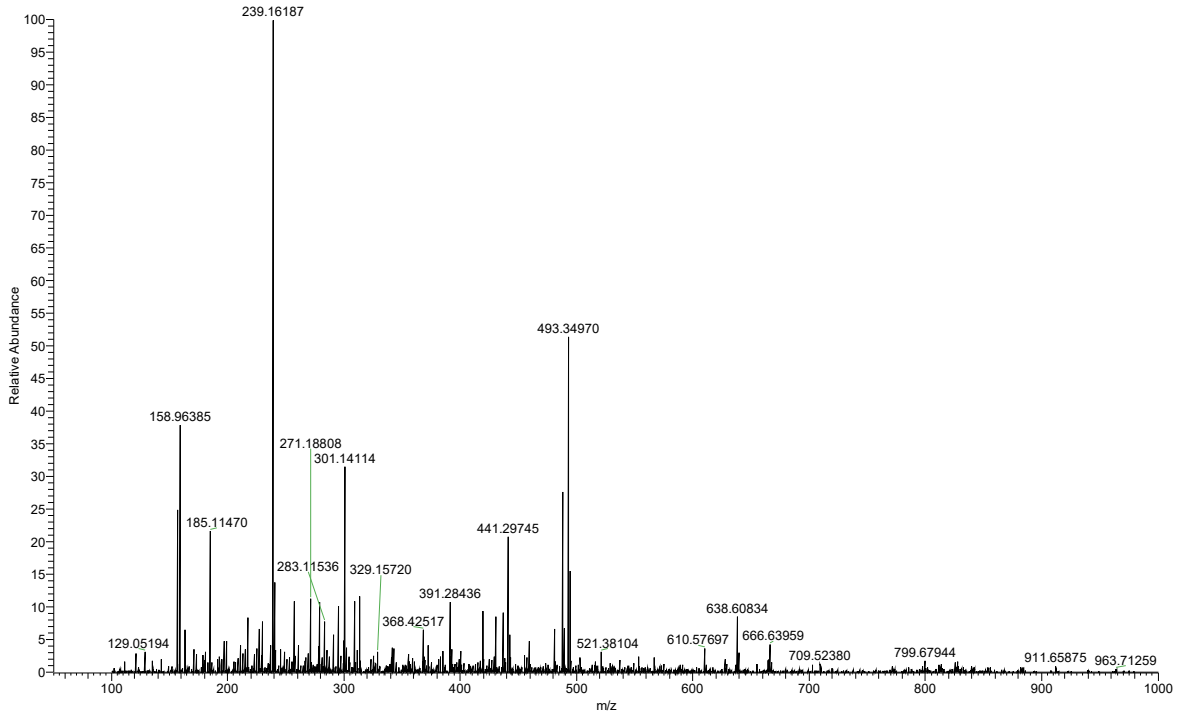

Fig. S67 HRMS spectrum (ESI, positive) of **PD2** heating at 270 ℃ under nitrogen atmosphere.

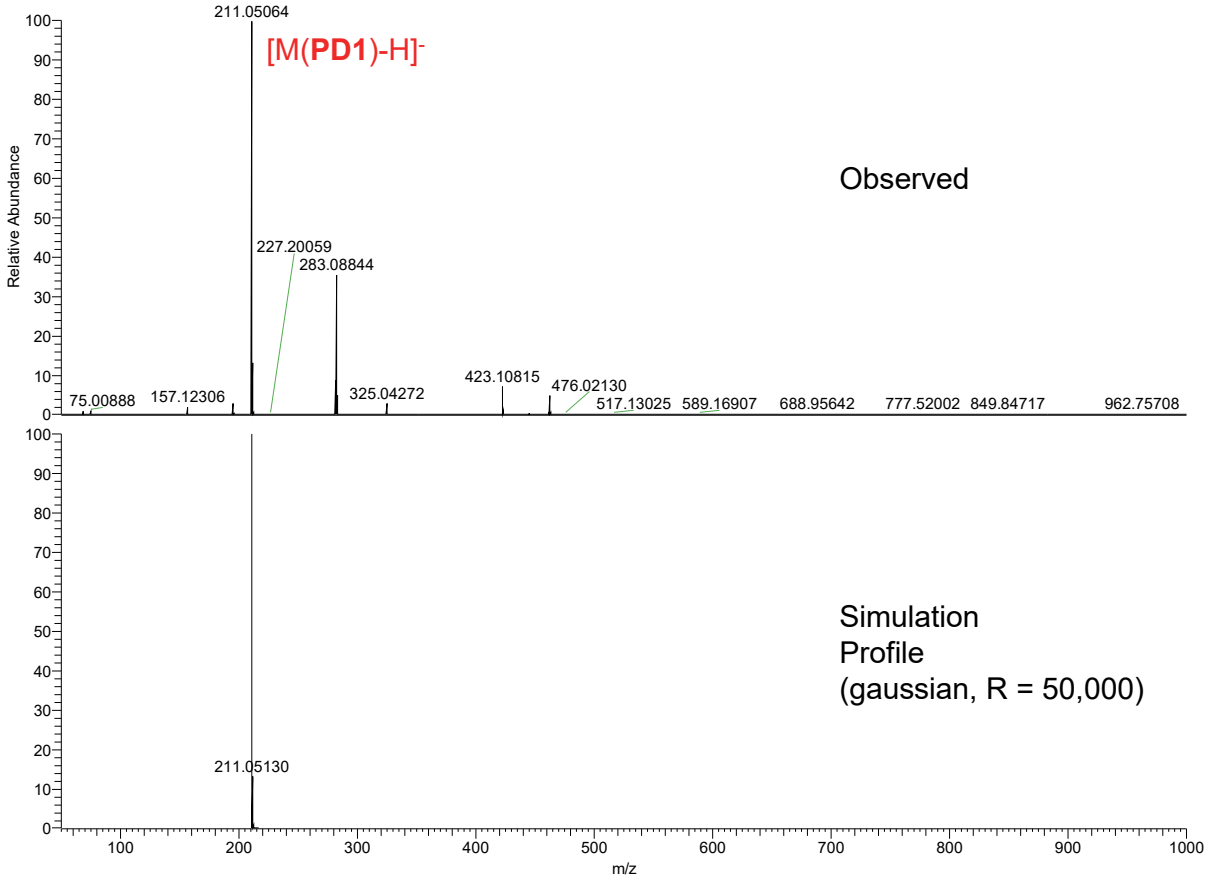

Fig. S68 HRMS spectrum (ESI, negative) of **PD1**.

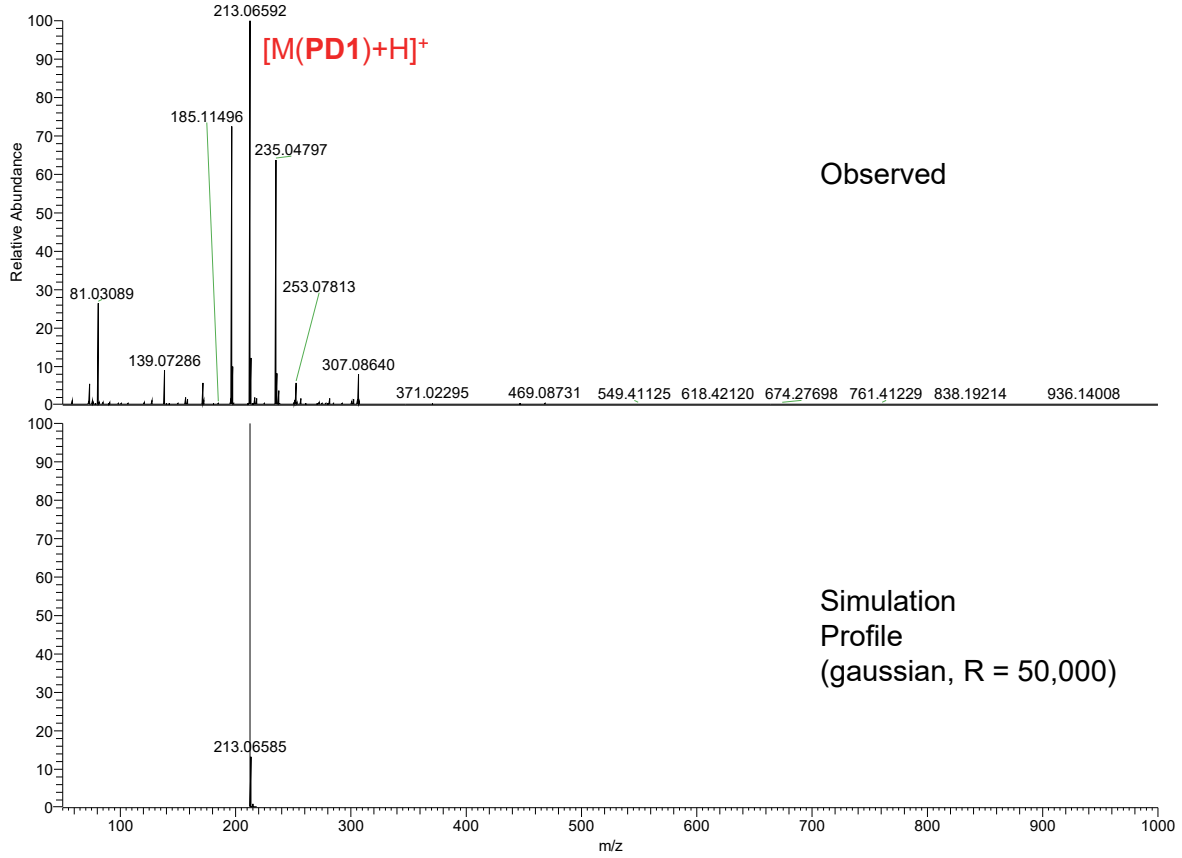

Fig. S69 HRMS spectrum (ESI, positive) of **PD1**.

10. Supporting References

S1. K. Ohira, M. Yamamoto, K. Imato and Y. Ooyama, *New J. Chem.*, 2023, **47**, 2711–2718.

S2. Gaussian 16, Revision B.01 and C.01, Gaussian, Inc., Wallingford CT, 2016.

S3. K. Ogawa, M. Miura, T. Nakayama and J. Harada, *Chem. Lett*., 2003, **32**, 840–841.